9-315-27660-9

National Library of Canada / Bibliothèque nationale du Canada

Canadian Theses Division / Division des thèses canadiennes

Ottawa, Canada
K1A 0N4

67667

PERMISSION TO MICROFILM — AUTORISATION DE MICROFILMER

- Please print or type — Écrire en lettres moulées ou dactylographier

Full Name of Author — Nom complet de l'auteur

James William Bentley Allwright

Date of Birth — Date de naissance

November 26, 1956

Country of Birth — Lieu de naissance

Canada

Permanent Address — Résidence fixe

175 Queen Victoria Dr.
Unit 93
HAMILTON, Ontario. L8W 1W6

Title of Thesis — Titre de la thèse

The Development of CCD Image Processing Techniques and Their Application to Surface Photometry of NGC 6166

University — Université

Saint Mary's University

Degree for which thesis was presented — Grade pour lequel cette thèse fut présentée

Master of Science

Year this degree conferred — Année d'obtention de ce grade

1985

Name of Supervisor — Nom du directeur de thèse

Dr. G. A. Welch

Permission is hereby granted to the NATIONAL LIBRARY OF CANADA to microfilm this thesis and to lend or sell copies of the film.

The author reserves other publication rights, and neither the thesis nor extensive extracts from it may be printed or otherwise reproduced without the author's written permission.

L'autorisation est, par la présente, accordée à la BIBLIOTHÈQUE NATIONALE DU CANADA de microfilmer cette thèse et de prêter ou de vendre des exemplaires du film.

L'auteur se réserve les autres droits de publication; ni la thèse ni de longs extraits de celle-ci ne doivent être imprimés ou autrement reproduits sans l'autorisation écrite de l'auteur.

Date

August 2, 1985

Signature

JWB Allwright

THE DEVELOPMENT OF CCD IMAGE PROCESSING TECHNIQUES AND THEIR APPLICATION TO SURFACE PHOTOMETRY OF NGC 6166

by

J. W. B. Allwright

A thesis submitted in partial fulfillment
of the requirements for the degree of

Master of Science

Department of Astronomy

Saint Mary's University

July 1985

Signatures of the Examining Committee

Gary A. Welch

G. A. Welch, Supervisor

G.F. Mitchell

G. F. Mitchell

B. C. Reed

B. C. Reed

D. G. Turner

D. G. Turner

Abstract

The Development of CCD Image Processing Techniques and Their Application to Surface Photometry of NGC 6166

by

J. W. B. Allwright

July 29, 1985

A systematic procedure for processing and reducing CCD-generated images has been developed. It involves removing unwanted objects and blemishes, subtracting the bias offset, removing the thermal background, correcting for areal sensitivity variations, and removing the sky background. This procedure has been applied to images of the cD galaxy NGC 6166 in Abell cluster 2199. Surface brightness profiles in B and R and a (B-R) colour profile have been generated for NGC 6166. Between 15 and 45 kpc the surface brightness profiles agree with the data of Oemler (1976), but beyond 45 kpc our profiles decline rapidly. The (B-R) colour profile shows that the galaxy becomes bluer by 0.03 mag between galactocentric distances of 15 and 33 kpc in agreement with previous observations. These results are tentative, pending improvement of our method of determining the sky background and examination of the complete set of data.

TABLE OF CONTENTS

List of Figures

List of Tables

Acknowledgements

I would like to thank Dr. Gary Welch for suggesting this topic, allowing me to use his data, and supplying much needed advice and encouragement over the past two years. I would also like to thank Drs. David Turner, George Mitchell, and Cameron Reed for reading (and surviving) the first draft, providing helpful comments, and participating in the defense process. Thanks go to Dr. John Kormendy for advice on image processing, to Dottie Welch for assistance with programming and to Laurie Reed for providing moral support. And last, but certainly not least, I thank my wife, Debbie, whose support, encouragement, and love made this thesis possible.

CHAPTER 1

INTRODUCTION

The term 'cD' galaxy was introduced by Matthews, Morgan, and Schmidt (1964). The 'cD' designation was based on Morgan's (1958) classification scheme in which a D galaxy was defined as having an elliptical-like nucleus surrounded by an extensive envelope. The D-like galaxies observed by Matthews, Morgan, and Schmidt had significantly larger and more diffuse envelopes than were typical of D galaxies. These large D galaxies were given the prefix 'c' in analogy with the notation for supergiant stars in the Henry Draper spectroscopic classification scheme. Therefore, 'cD' galaxy reads as, 'supergiant D' galaxy.

cD galaxies are the largest, most luminous, and most massive galaxies known. Their absolute visual magnitudes range from -23 to -26, and their masses are of the order of 10^{13} $M_{\odot}$ (Jenner 1974). All known cDs are located in clusters of galaxies, and are usually near the cluster's projected centre.

Lists of cD candidates have been compiled by Matthews, Morgan, and Schmidt (1964, 10 galaxies), and Morgan and Lesh (1965, 18 galaxies). Morgan, Kayser, and White (1975) and Albert, White, and Morgan (1977) extended the search to poor clusters (those not listed in Abell's 1958 catalogue), and found a total of 23 possible cDs. Valentijn and Bijleveld (1983) have compiled a list of 104 cD candidates, which includes the earlier lists as well as cDs associated with X-ray sources. Cluster classification schemes which have a distinct class for clusters containing cDs, such as the schemes of Bautz and Morgan (1970) and Rood and Sastry (1971), also generate lists of cD candidates (cf., Leir and van den Bergh 1977, Rood and Sastry 1971).

Photographic surface photometry of cDs (e.g. Oemler 1973, 1976; Thuan and Romanishin 1981; Morbey and Morris 1983; and Valentijn 1983) has shown that these galaxies possess extensive diffuse halos. DeVaucouleurs (1948) and King (1966) laws can be successfully fit to the inner regions of cDs, but the halos tend to be much brighter than the predictions of these models. The luminosity of the halos of cDs correlates strongly with total cluster luminosity, the correlation being stronger for cDs in rich clusters than for those in poor clusters. This is interpreted as evidence that the cluster environment has had some effect on cD formation, especially the halo.

Studies of colour gradients in cDs (Gallagher, Faber, and Burstein 1980; and Valentijn 1983) show that cDs have steeper colour gradients than do normal ellipticals (Strom and Strom 1978a, b, c). In cDs the changes in (B-V) from the nucleus to 50 kpc from the centre range from 0.1 to 0.6 mag, whereas in normal ellipticals it is usually less than 0.1 mag. These gradients need more detailed study so that reliable comparisions can be made with the predictions of cD galaxy formation hypotheses.

Normal galaxies are believed to form by contraction of a protogalactic mass in either a quasi-static or free-fall mode. These modes apply to masses less than $10^{12}\ M_{\odot}$. Therefore, if cDs are indeed of the order of $10^{13}\ M_{\odot}$, then these formation mechanisms are not necessarily applicable (Rees 1985). This would present difficulties for theories which postulate that cDs are the extension of the bright end of the galaxy luminosity function. Three alternative formation mechanisms have been proposed and are discussed briefly below.

The cannibalism (or merger) model (Ostriker and Tremaine 1975; Ostriker and Hausman 1977; and Hausman and Ostriker 1978) proposes that dynamical friction between galaxies causes them to lose kinetic energy and fall to the centre of the cluster potential well. The galaxies merge there and are eventually joined by other cluster members. As the central galaxy grows by accreting its smaller neighbours, it develops an extended diffuse halo and takes on the appearance of a cD. It is predicted that the merger of galaxies will result in a homogenous mixture of stars with little or no radial colour changes.

The tidal debris model (Richstone 1975, 1976) proposes that collisions between galaxies result in the removal of material from their halos. This material falls to the centre of the cluster and forms a diffuse halo around an existing central galaxy. Since the infalling material is bluer than the existing central galaxy, the resulting cD will have a radial colour gradient.

The cooling intracluster medium (ICM) model (Fabian and Nulsen 1977; Fabian, Nulsen, and Canizares 1982; Cowie and Binney 1977; and Sarazin and O'Connell 1983) suggests that the observed X-ray emission from the central regions of clusters (Jones and Forman 1984; and Stewart et al. 1984) in excess of that expected from models of a hot 10^{8} K ICM is due to the presence of cooling gas in these regions. The pressure of the surrounding hot gas drives the cooler gas inward, resulting in a large-scale mass inflow. The X-ray data suggest mass inflow rates as great as 400 $M_{\odot}$ yr^{-1}, which over 10^{10} yr could result in the accumulation of 4×10^{12} $M_{\odot}$ - equivalent to a galaxy (Stewart el al. 1984). It is proposed that the gas cools sufficiently that fragmentation occurs, resulting in the optical filaments reported by Fabian et al. (1981) and Heckman (1981). Further cooling and fragmentation eventually allows stars to form. The conditions in the filaments are such that the upper mass cutoff of the initial mass function may be as low as 1 $M_\odot$, resulting in a population of faint red stars (Sarazin and O'Connell 1983). This model predicts that the halo should be roughly 0.2 mag bluer in (U-V) than the inner regions.

cD galaxies are intrinsically very luminous and as such are useful as standard candles in cosmological tests. According to most theories of their origin, they are also useful as probes of dynamical evolution within clusters of galaxies. However, their usefulness is reduced by our limited understanding of how evolution affects their observable parameters. Studies of the distribution of light in cDs, especially in more than one bandpass, help to determine how cDs evolve. The primary aim of this study was to obtain a better understanding of the radial surface brightness and colour distributions of the cD galaxies in Abell clusters 2199 and 1413 (hereinafter A2199, A1413). It was hoped that these distributions, especially the colour data, could be used to test the models discussed above. This thesis involved 1) the development of a systematic procedure for processing and reducing CCD images, and 2) the generation of normalized surface brightness and (B-R) colour profiles for the cD galaxy NGC 6166 in A2199. It should be stressed that the reduction procedure was developed for surface photometry only - not stellar photometry. Problems were encountered in dealing with fluctuations in the sky background. Delays as a result of these problems did not allow the completion of processing of the A1413 images or the calibration field images.

Chapter 2 describes the equipment used, the programme galaxies, and the observing procedure, and reviews CCDs, their operation, and the types of images they generate. Chapter 3 is a discussion of the specific procedure developed here for CCD image processing. Chapter 4 contains a description of the method of generating surface brightness profiles, and a comparison of the results with previous work and theoretical predictions. Chapter 5 summarizes the results and the appendix contains a journal of observations.

CHAPTER 2

DATA AQUISITION

2.1 Equipment

The observations described here were obtained on 3/4 and 4/5 May 1984 by Dr. G. Welch using an RCA CCD camera at the prime focus of the Canada-France-Hawaii (CFH) telescope. The 3.58m (usable diameter) primary mirror has a focal length of 13.53 m. The prime/coude upper end was used with the wide field corrector, giving an f/ratio of 4.20. The scale for this configuration is 13.89 arcsec/mm (Racine and Lelievre 1982).

The detector used was an RCA SID53612 charge-coupled device (CCD) camera. The CCD is a thinned backside illuminated chip with an imaging area of 512×320 (= 163,840) picture elements (= pixels). The pixels are 30μm square and are on 30μm centres. The scale given above corresponds to 0.417 arcsec/pixel giving sky coverage of roughly $3'.56 \times 2'.22$. The detector's sensitivity as a function of wavelength is given in figure 2.1.

The filters used were Mould's B and R with effective wavelengths and FWHM respectively of 4420 Å, and 1129 Å in B and 6485 Å, and 1267 Å in R (Christian 1984). The filter transmission curves are given in figures 2.2 and 2.3.

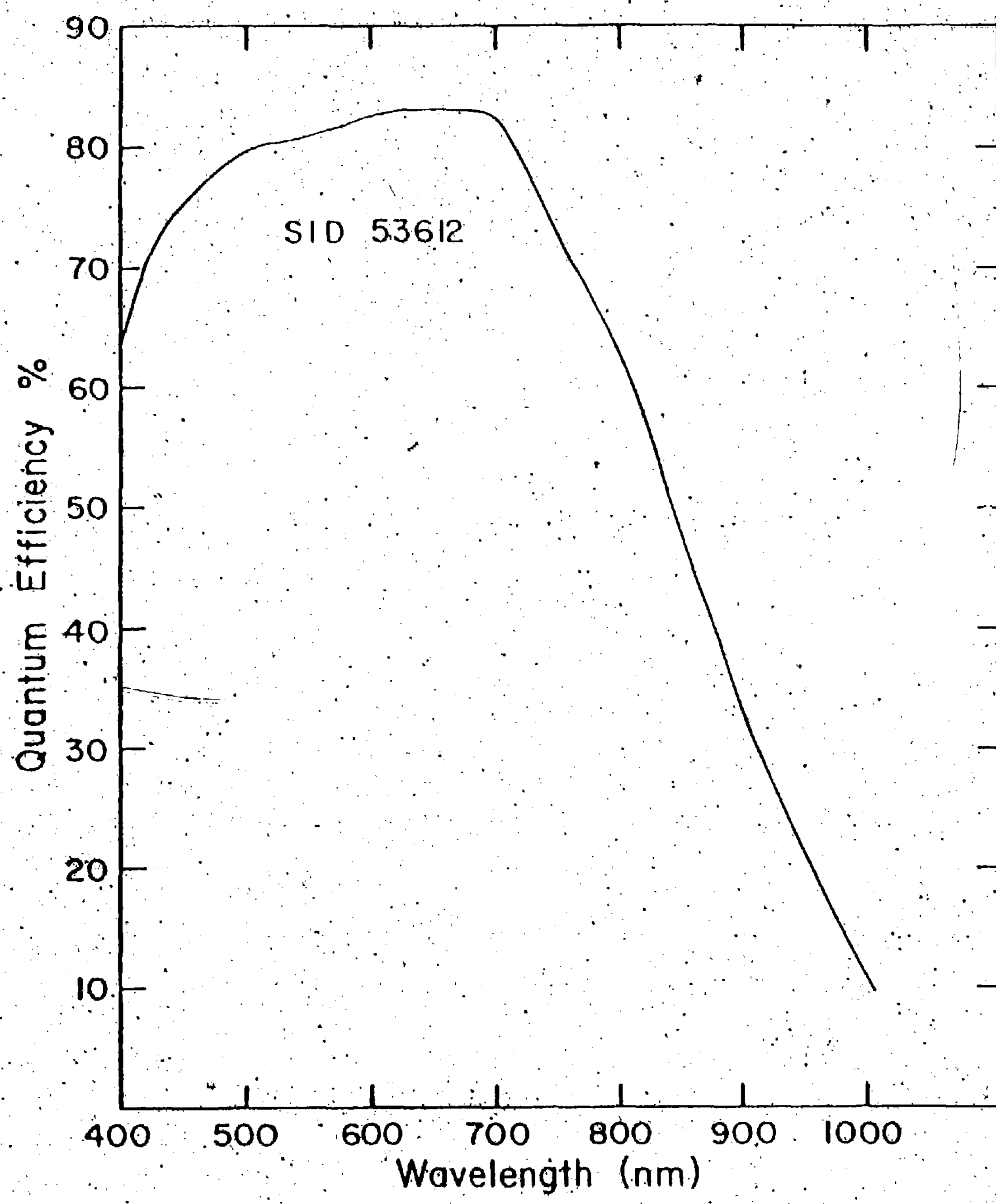

Figure 2.1. The response curve for the RCA SID53612 CCD (Christian 1984).

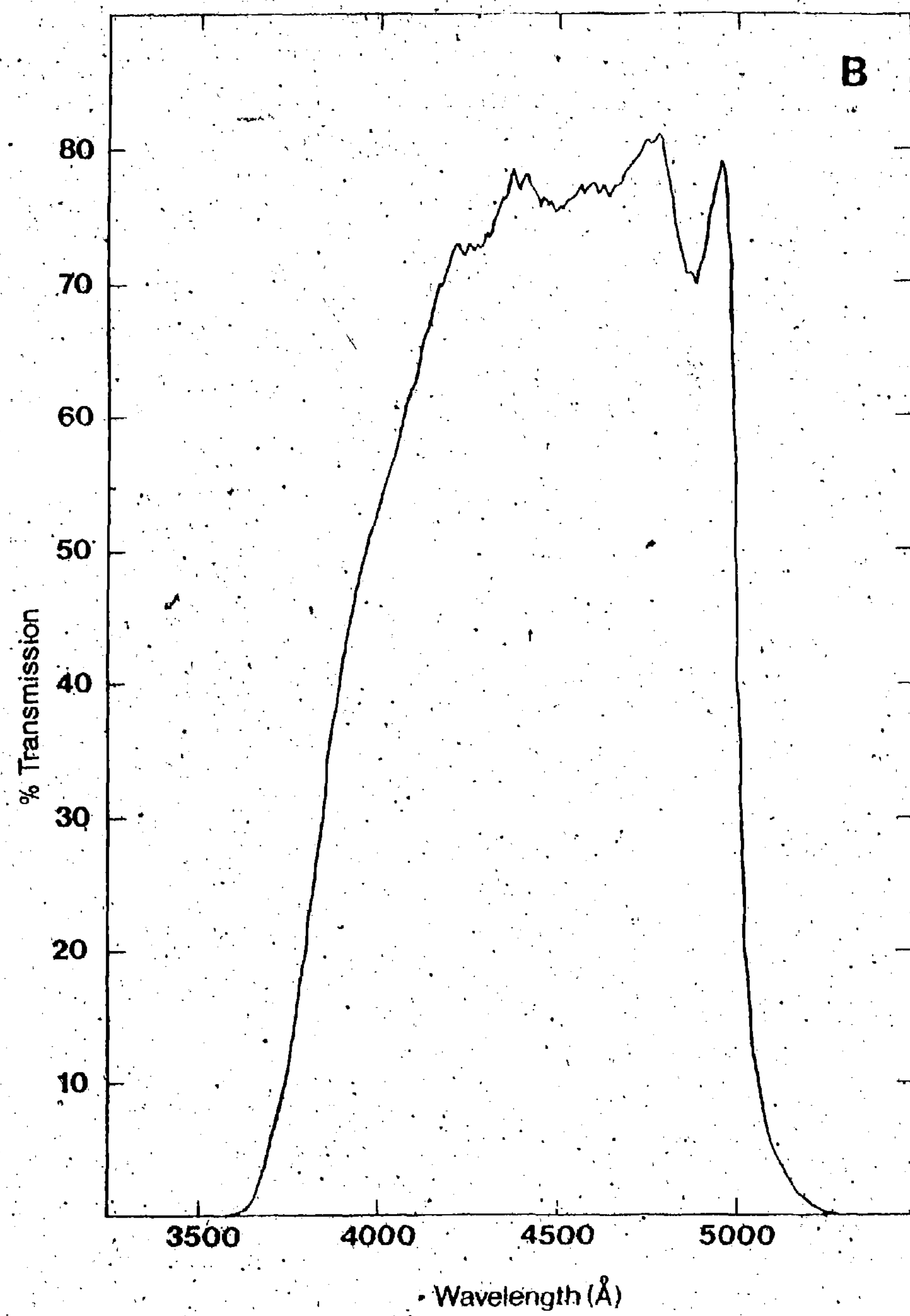

Figure 2.2. The transmission curve for the B filter (Christian 1984).

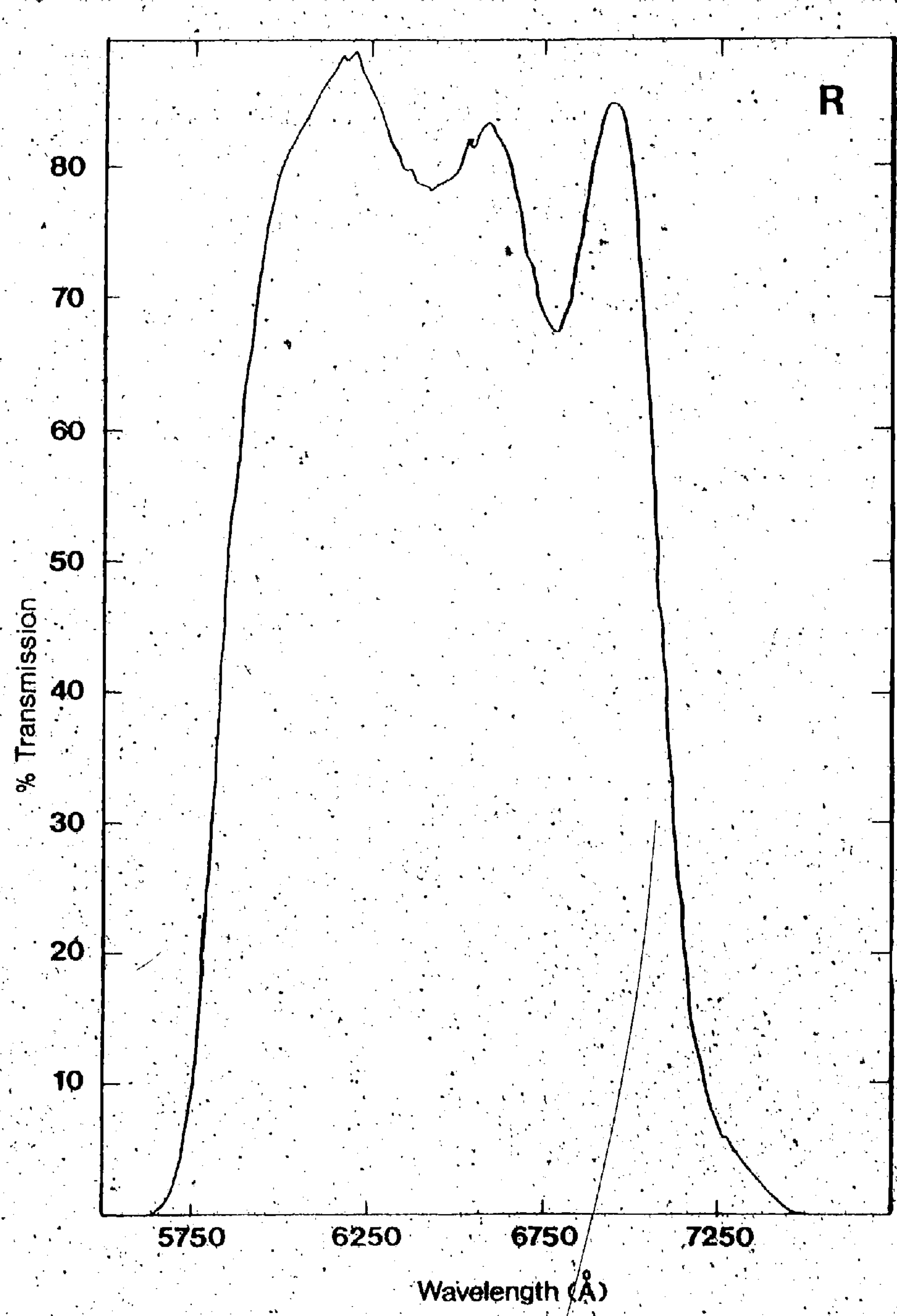

Figure 2.3. The transmission curve for the R filter (Christian 1984).

2.2 Programme

The programme objects consist of NGC 6166 in A2199 and the anonymous cD in A1413. These galaxies are well established as being cDs on the basis of existing surface photometry (Thuan and Romanishin 1981, figure 7). Their surface brightness profiles display large departures from deVaucouleurs laws fit to their inner regions, in the sense that for a given radial distance the galaxy is actually much brighter than predicted by the fit. These departures occur close to the centres of these galaxies, which makes them easier to detect and study. Both galaxies are known to have multiple nuclei: NGC 6166 has 4, and the A1413 cD has at least 2. The presence of multiple nuclei may indicate that mergers have occurred recently. Characteristics such as these make these galaxies excellent examples of the cD phenomenon and prime candidates for study.

Existing photometry will provide a valuable check on our reductions. NGC 6166 and the cD in A1413 have been studied in detail by Oemler (1976). NGC 6166 has also been studied by Minkowski (1961), Gallagher et.al. (1980), and Murphy et.al. (1983). The surface brightness profiles of Oemler (1976) (as presented in Thuan and Romanishin 1981) and the colour profiles of Gallagher et al. (1980) and Valentijn (1983) will be used for comparison with the results of this study.

2.3 Introduction to CCDs

The following is a simplified description of CCDs, based on RCA's design. A CCD consists of a layer of n-type silicon (substrate) in which thin strips of p-type material known as channel stops are embedded. The substrate is covered with an insulating layer of oxide. Electrodes, in the form of thin strips oriented perpendicular to the channel stops, are deposited on the oxide layer. Potential differences are applied to the electrodes to form potential wells in the silicon substrate. A picture element (hereinafter pixel) is formed by two channel stops and a set of three electrodes in which the central electrode is at a higher positive potential relative to the two outer electrodes, thus creating a potential well under the central electrode. The channel stops form 320 rows and the electrodes form 512 pixels per row, therefore the CCD contains 512 X 320 = 163,840 pixels (see figure 2.4).

Electrons in the valence band are raised to the conduction band by the absorption of energy from photons incident on the silicon substrate. In the conduction band the electrons are attracted to the potential well under the central electrode of each pixel. During integration the potentials are fixed and electrons accumulate in the potential wells in direct proportion to the number of photons striking the silicon in their vicinity. Therefore, each pixel contains information on the intensity of the source at its location. This information is collected by the process of reading-out the chip, which involves increasing the potential of the bounding electrode closest to the output register, and decreasing the potential of the central electrode. The potential well and the electrons it contains are now underneath the bounding electrode. When these changes in potential occur three times the potential wells and electrons move the length of one pixel, and the first column of 320 pixels moves into the output shift register. The output shift register is a column of pixels like any other, but it does not form part of the image area and is only used in the read-out process. It is located to the left of the image area on a displayed image (see figure 2.4). Before the next column is shifted, each pixel of the output shift register is transfered to an on-board pre-amplifier by the same method as outlined above. The electrons stored in each potential well produce an analog signal, which is converted to a digital number by external electronics. This information, in analog-to-digital units, hereinafter ADU, can be manipulated and stored by a computer. When all 320 pixels have been read, the next column of the image is shifted into the output shift register and the process is repeated. This continues for 512 columns and results in a set of 163,840 numbers which represent the image.

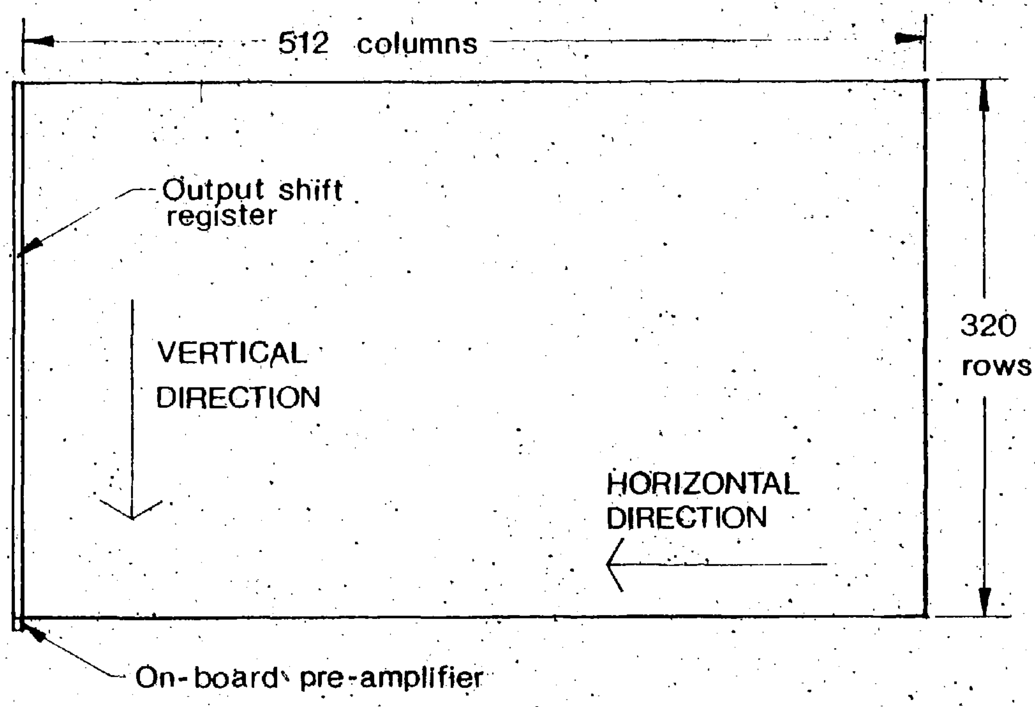

Figure 2.4. A schematic diagram of the RCA CCD showing the horizontal and vertical directions as used in the text. Note that in RCA's documentation these directions are interchanged. The horizontal direction corresponds to the direction of electron motion in the image area. The vertical direction corresponds to the direction of electron motion in the output shift register.

The names given to the various types of frames or images are: bias frames, dark frames, dome flat-field frames, sky images, and object images. A bias frame is obtained by reading-out the chip a few times) and then immediately reading it out again without any exposure to light, and with as little time elapsed since the end of the last cleaning as possible. This signal approximately represents the offset introduced by the electronics during read-out. The bias level actually consists of a fixed areal pattern, represented by the bias frame, added to a variable (from frame-to-frame) offset. This variable offset is represented by the mean of an overclocked area which will be described below. All other data frames must have a bias level subtracted (pixel-by-pixel) from them.

A dark frame is an integration (of 900 seconds in this case) without exposure to light. The signal is due to the accumulation of thermal charge in the potential wells. No matter how cold the chip is maintained (near -110°C for the present observations) a few electrons will have sufficient energy to occupy the silicon conduction band. These electrons are present whether or not the chip is exposed to light. The contribution of these electrons to the total signal must be removed from other frames. This is accomplished by subtracting (pixel-by-pixel) a dark frame scaled to the exposure length of the frame being treated. The scaling is required because the dark signal is a function of time. This procedure assumes that the temperature of the chip remains sufficiently constant ($\pm 1\,^{\circ}C$) throughout the observing run.

A dome flat-field frame is obtained by a short integration (60 - 90 seconds) of a smooth flat white painted surface on the interior of the dome which is illuminated by a high intensity lamp. It is assumed that the true image is areally uniform (flat) because the source is far out of focus. Therefore, within random error, each pixel receives the same number of photons. If the CCD were perfect, each pixel would output the same signal (within the random error). The dome flat-field is a measure of how the actual sensitivity of the chip varies from pixel to pixel. The method of using dome flat-field frames to partially remove sensitivity variations will be discussed in section 3.5.

The sky images are obtained by exposing the CCD to a relatively empty region of sky. The exposure times are the same as those of the object images in the corresponding filter. In this study the sky fields are between 5′ and 30′ north or south of the object image fields. Inevitably these empty regions have numerous faint stars and galaxies which must be removed to make the image useful.

The purpose of the sky images is two-fold. First, the dome flat-field frames do not remove all the effects of pixel-to-pixel sensitivity variation across the chip. This sensitivity variation is a function of the spectral energy distribution of the source. The high intensity lamp and the sky do not have the same spectral energy distributions, therefore the response of the CCD to the two sources is not the same, and flat-fielding with the dome images will not completely remove the effects of sensitivity variation. The residual sensitivity variation is removed by a second flat-fielding operation using a suitably smoothed mean of the sky images.

Second, these images are also used to determine the sky background level appropriate to object images. An accurate determination is required because the halo brightness level is only a small fraction of the sky level.

Object images are exposures of the objects to be studied and of calibration fields. Integration times for the galaxies are 1200 seconds in B and 900 seconds in R. Each imaging sequence of the cDs consists of two images placed 'end-to-end' (with 1/4 overlap of the images along their long dimension) to cover the galaxy in the radial direction. The calibration fields, containing sequences of standard stars, are those in the globular clusters M92 and NGC 4147 (Christian et al. 1985). Exposures of these fields range from 60 to 120 seconds. These images will be used to determine the extinction and transformation coefficients.

Common to all images is an overclocked area. This area is obtained by continuing the chip read-out after the 512 columns containing the actual image data have been read and stored. On the CFHT CCD, the overclocked area consists of 13 columns of data. The process of obtaining the overclocked area effectively cleans out any 'leftover' electrons which might have spilled out of the potential wells during the readout. The signal in the overclocked area typically shows a sharp decline over the first 4 columns to a relatively constant level over the last 9 columns. These last 9 columns are used to fix the bias offset for each image by determining the average ADU/pixel value in the region between columns 517 and 525 and rows 2 and 319.

The general procedure followed during an observing session was to obtain a half dozen bias frames and dome flat field frames during twilight. After twilight a few images of a calibration field were taken, followed by the first part of a cD imaging sequence, consisting of: the central field of the galaxy in R, the corresponding sky in R, the same sky field in B, and the central field in B. This was followed by a few calibration field images and/or a few bias frames and the second part of a cD imaging sequence. This followed the same format as the first part, except that the field of view was offset within the galaxy as described above. The order of filter usage was not necessarily as specified above. When both galaxies had been imaged a few more calibration field images and bias frames were taken. At the end of the night the CCD camera was set to automatically obtain dark frames by performing repeated 900 second integrations with the shutter closed. Other dark frames were also obtained during the observing session. A detailed list of the observations is given in the Appendix.

CHAPTER 3

IMAGE PROCESSING AND DATA REDUCTION

The images generated by a CCD require a considerable amount of processing to render them useful for quantitative work. For example, surface photometry of diffuse objects may require that star images in the field be removed. The effect of pixel-to-pixel sensitivity variations in the CCD must be removed in order to accurately measure the light distribution in extended objects.

A computer system is used to perform all handling and manipulation of the image data. In this case the system is based on a DEC PDP 11/23 running under the RT-11SJ operating system. A Kennedy Model 9800 tape drive is used for archival storage of data. A DSD 880 31.1 Megabyte winchester hard disk is used for peripheral storage during processing. Display of images is accomplished with a Matrox 8-bit gray scale image display system and a TV monitor.

The image processing procedure consists of removing unwanted objects and blemishes (cleaning), removing the bias level introduced by the electronics (bias frame subtraction), removing the thermal background (dark frame subtraction), correcting for areal sensitivity variation (dome and sky flat-fielding), and removing the sky background. The images form a hierarchy in the sense that processing an image involves the use of all image types which preceed it in the hierarchy. The following is a list of the image types ordered according to the number of operations involved in processing them: bias frames, dark frames, dome flat-fields, sky images, and object images. Bias frames require cleaning and subtraction of the mean of the overclocked area. Dark frames require cleaning, overclock-subtraction, and subtraction of the bias frame. Dome flat-field frames require the same processing as the dark frames, as well as subtraction of a dark frame. Sky images require the same processing as the dome flat-fields, as well as flat-fielding using the dome flat-fields. Object images require the same processing as sky images, as well as sky flat-fielding and subtraction. These operations require the use of a large number of programmes which were written either individually or in groups by G. Collins, D. M. K. Welch, G. A. Welch, and the author. The reduction procedure took about a year to develop and represents the majority of the time spent on this thesis. For this reason, and because the procedure is not documented elsewhere, a fairly thorough description will be given. Section 3.1 gives a brief summary of the method of processing an object image (see also Figure 3.1). Section 3.2 describes the general methods of cleaning, and sections 3.3 through 3.7

describe the treatment of the various types of images. Table 3.1 gives descriptions of the functions of the various programmes. Listings of these programmes are available from Dr. G. A. Welch.

3.1 Summary of Image Processing

The following is a summary of the method of processing an object image using the software existing at the time of writing:

(1) Blemishes and objects larger than the filter to be used should be removed using programme FUZH and any hot rows or columns can be removed using programme CLEAN.

(2) Smaller blemishes can be removed using programme MEDFR with a filter size of 21 pixels, a discriminant of 20 ADU, and unit weights.

(3) The average of the overclocked area can be calculated using programme RECTH and subtracted from each pixel of the object image using programme ARITIR. This procedure removes the DC offset introduced by the electronics.

(4) A bias frame (or ideally a mean of many bias frames collected over the observing run) should be subtracted using programme SUBR. This will remove the fixed pattern of noise introduced by the electronics during read-out.

(5) An appropriately scaled dark frame (or mean dark frame) should be subtracted using programme SUBR. This will remove the thermal background.

(6) First order sensitivity variations can be removed by flat-fielding with an average dome flat-field using programme FLATR.

(7) Residual sensitivity variations can be removed by flat-fielding with a cleaned mean sky (possibly smoothed by averaging in blocks using programme BLKAVG)

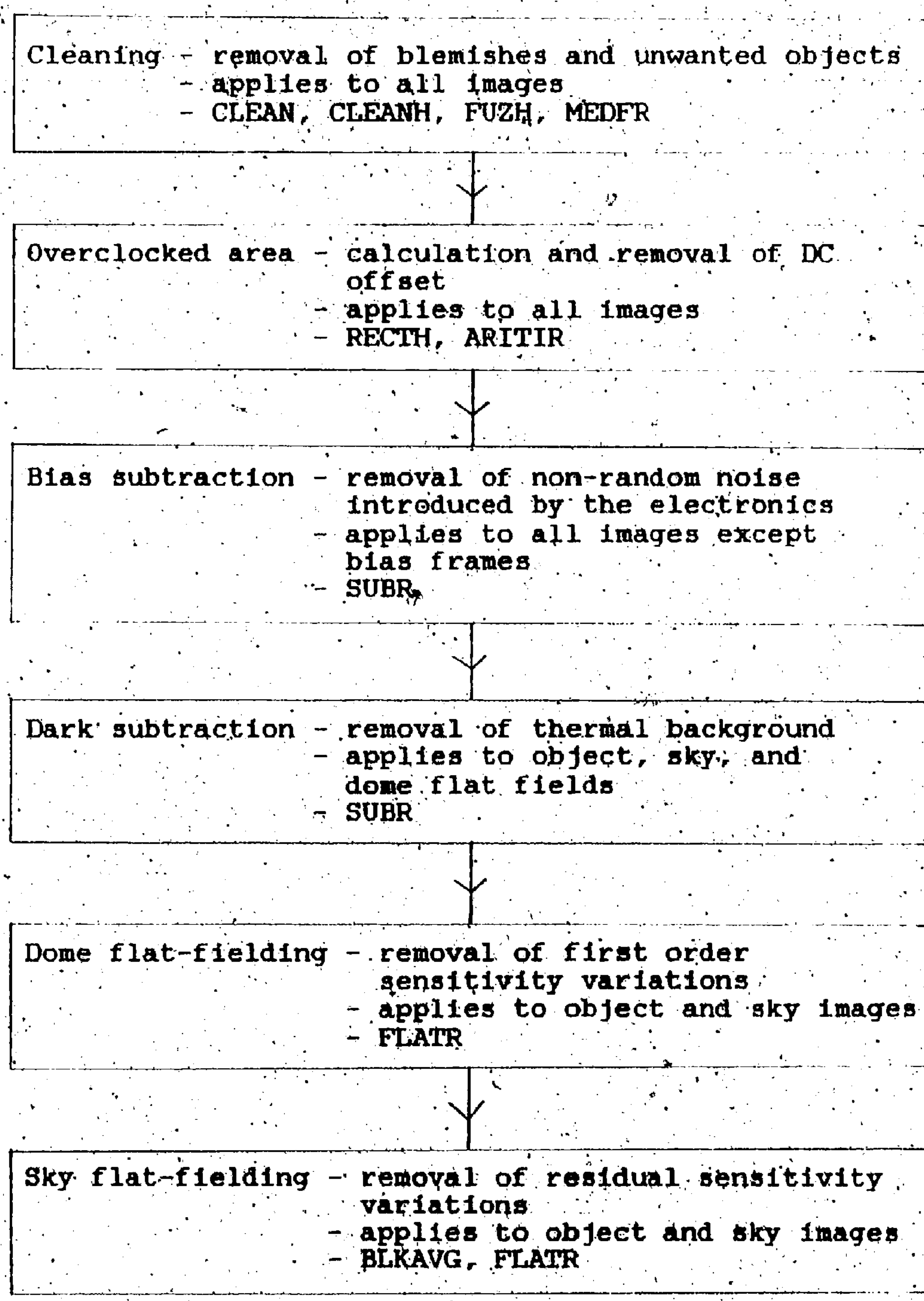

Figure 3.1. A flowchart of the various stages of image processing, including the types of images each stage applies to, and the programmes used at each stage.

3.2 Image Cleaning

All CCD images suffer from cosmetic flaws. These may be caused by rows or columns of pixels or single pixels which do not behave 'normally', in that they do not respond to photons in a manner similar to the majority of pixels. Some areas of the chip may be completely 'dead', rendering one or more pixels insensitive to light. In contrast, some areas 'bloom', that is they produce a signal larger than the background with or without exposure to light. In its milder forms this latter problem results in a bright spot (similar in appearance to a stellar image) often called an LED (light emitting diode). In more severe cases it can result in a hot row created by smearing the excess electrons along the row during readout.

Another problem results from cosmic ray events. These produce hot spots or streaks (depending on the angle of incidence) comprising as many as 8-10 pixels. The cosmic rays responsible are probably muons and electrons with energies in the 10 to 10^3 MeV range, which deposit some of their energy in the silicon substrate by exciting and ionizing silicon atoms (Leach and Gursky 1979). Cosmic rays are incident at a rate of roughly 0.08 $cm^{-2} s^{-1}$, which for a chip 1.47456 cm^2 results in 420 events hr^{-1}. The majority of events cause minor blemishes which are lost in the noise. Typically 8-10 cosmic ray blemishes were removed on each image. This type of blemish is found on all images except the bias frames.

Astronomical objects that are not part of the programme need to be removed. These occur only on sky and object images and on average in roughly equal numbers.

A number of programmes were developed to remove these unwanted objects and blemishes. The most straightforward of these was programme CLEAN. This is an interactive programme, which is used to replace a specific area of the image, usually part of a few rows or columns, with either a specified value or a value interpolated in one dimension from the pixels bordering the area. This programme was usually used to remove hot rows in overclocked areas.

Programme CLEANH was developed for the purpose of automatically removing single pixels and small groups of pixels (up to 4-6 pixels) which differ from the local background by more than some discriminant. The discriminant can be a multiple of the standard deviation of the ADU/pixel value in some area of the image, or its value can be specified by the user. The method is to compare a pixel with its immediately adjacent neighbours. If the absolute value of the pixel differs from the local background by more than the discriminant then it is replaced by the local background value. The local background value is calculated from the previous background and a weighted mean of the surrounding pixels from which the central pixel differed by more than the discriminant. A rapid increase in ADU/pixel values was found in the upper- and lower-most rows of all images. This posed a problem because CLEANH treated these rows as hot and attempted to clean them. The problem was solved by having the programme ignore the upper and lower 10 rows of the image. The first 16 columns presented a similar problem and these were also ignored. The programme can also ignore specified rectangular areas of the image. This option was developed for use on the dark frames.

CLEANH cannot remove blemishes larger than 4-6 pixels square because in these cases the pixels used for comparison are not representative of the local background. Although CLEAN can remove larger blemishes it is restricted to an interpolation in one dimension. The highly interactive programme FUZH was developed to overcome these limitations. The user specifies the parameters of an ellipse to be drawn around the object to be removed. A square box is then drawn around the ellipse. A least-squares fit of a two-dimensional linear function is made to the region between the ellipse and the box, and is used to interpolate over the area contained within the ellipse. The user can graphically check whether the feature has been satisfactorily removed, and if desired store the changes in a new file. The interpolations appear as obvious modifications on the TV monitor, but it is the lack of random noise in the interpolations which gives the cleaned areas their strikingly smooth appearance.

FUZH and CLEANH tend to be rather time-consuming (up to 4 hours per image on our system), and CLEANH's method of determining whether a pixel should be cleaned is more complicated than necessary. To speed up the cleaning process we developed programme MEDFR which uses the technique of the weighted median filter (Brownrigg 1984). This programme eventually replaced CLEANH and to a large extent FUZH because it is capable of removing blemishes in a large range of sizes. It is also fully automatic and therefore requires less processing time (~30 minutes). The method consists of examining a set of 9 pixels at the corners and midpoints of a square, the size of which is an odd integer specified by the user. This set of 9 pixels forms the filter. The programme finds the median value of the 9 pixels and replaces the central pixel with the median if it differs from the median by more than a specified discriminant. The 9 pixels can be weighted when determining the median. This programme can completely remove any blemish smaller than the filter; however, a border around the image of width equal to half the filter size will not be cleaned. The detailed cleaning procedure for each type of image will be discussed in the appropriate section below.

3.3 Bias Frames

As mentioned previously, bias frames are essentially zero second integrations representing the offset level introduced by the electronics during the read-out process. The first step in the treatment of the bias frames was to use programme RECTH (which performs various statistical computations within a specified rectangular area) to determine the typical ADU value of these images, the numbers and types of hot spots, and the size of any large scale gradients. A vertical cut through a typical bias frame showed a rapid drop over the first 100 rows (from 476-456 ADU) and a decrease of 2 ADU from row 101 to 320. This vertical gradient is believed to be due to the synchronization of the read-out of the output shift register with the ambient 60 Hz frequency. There was no noticable overall horizontal gradient. The overclocked area showed none of the hot rows or gradients found in other images.

A number of bias frames were examined to obtain some idea of the typical signal to be found in these images. Typical values range from 453 to 457 ADU/pixel. The frames were examined using the byte selection option of programme DISH (used to display images on a TV monitor) to locate extremely hot pixels ($\pm$ 32000 ADU).

Programme CLEANH was used to remove these hot pixels using a discriminant of 10 times the standard deviation determined in the 51 X 51 pixel box defined by columns 200 and 250, and rows 150 and 200. The standard deviation typically found was between ±3.1 and ±3.4 ADU; therefore, the discriminant was between 31 and 34 ADU. Typically 1 or 2 extremely hot pixels were found per image.

A mean value for the overclocked areas was determined using programme RECTH with a rectangle defined by columns 513 and 525, and rows 2 and 319. The upper- and lower-most single rows were excluded because they were abnormally high. The mean determined within this rectangle was subtracted from each pixel of the frame. This was done separately for each bias frame using programme ARITIR. These frames will be referred to as overclock-subtracted frames.

Once all the bias frames from both nights were overclock-subtracted they were combined using programme AVR to produce a mean bias frame (file: B001CM). The average signal of the mean bias frame was -0.35 ADU. This mean bias frame is assumed to represent an underlying areal structure common to all images. Added to this structure is the variable offset represented by the mean of the overclocked area of each image. The offset is variable in the sense that it is unique for each image.

3.4 Dark Frames

The dark frames are 15 minute integrations without exposure to light, and represent the thermal charge accumulated during an integration of equal length. The most striking aspect of these frames is the appearance of bright spots at the same locations in all the frames. These are the LEDs referred to previously. They are caused by the diffusion of electrons from the valence band into the potential wells in the conduction band. The accumulation of electrons in these areas mimics the effect of photons incident on the areas during integration.

At the suggestion of Kormendy (1984) we did not remove the LEDs in the dark frames, since they ought to be removed from other frames when the mean dark frame was subtracted. To do this we needed to locate the bright spots common to the 29 usable dark frames. Programmes HUNTH and PIXH were written for this purpose. HUNTH uses CLEANH's detection code, but instead of replacing the detected hot pixels it merely stores their coordinates in a file. PIXH then searches the files created by HUNTH (one file per frame) to locate pixel coordinates which are common to all frames. Only those pixels which are bright in all frames are defined as LEDs. A discriminant of 15 ADU, which is approximately 5 times the standard deviation of the noise, was used in HUNTH. A total of 60 pixels, forming 16 groups of 1 to 30 pixels, were found to be common to all 29 dark frames.

A rectangle was placed around each group of bright pixels and CLEANH was modified so that it would not operate inside the boundaries of the specified rectangles. CLEANH was run on all dark frames using ARCH1.DAT with a discriminant of 15 ADU and the upper and lower 10 rows skipped. Typically 180-220 bright pixels were found per image.

Examination of the overclocked areas of the dark frames typically showed a decline over the first 4 columns (513-516), from the image area value of ~459 ADU/pixel to the typical overclocked area value of ~454 ADU/pixel. In determining the average of the overclocked area the first four columns were avoided by using a rectangle defined by columns 517 to 525 and rows 2 to 319 (hereinafter called the standard rectangle). The mean generated from within this rectangle was subtracted from each pixel of the corresponding image generating an overclock-subtracted dark frame. The set of 29 overclock-subtracted dark frames from both nights was combined to produced a mean overclock-subtracted dark frame.

Areal variation of the bias level was removed by subtracting the mean bias frame from the mean overclock-subtracted dark frame using programme SUBR (which subtracts two images pixel-by-pixel). This produced the mean bias- and- overclock-subtracted dark frame (file; D001CB).

The accumulation of thermal charge is assumed to be a linear function of time, so that dark frames corresponding to different integration times can be constructed from the mean dark frame simply by multiplying by the ratio of the integration times. For example, the mean dark frame for B object images which have integration times of 1200 seconds would be equal to the original mean dark frame (D001CB) multiplied by (1200/900).

3.5 Dome Flat-Field Frames

The dome flat-field frames are exposures of 60 seconds (in R) or 90 seconds (in B) of a white screen attached to the inside of the dome. The only remarkable thing about them is their high signal, typically of the order of 10^4 ADU/pixel.

The dome flat-fields were processed with CLEANH using a discriminant of 1500 ADU (=50σ to 300σ) and with the upper and lower 10 rows skipped. Examination of the overclocked area showed visual evidence of hot rows. In most images these were found at rows 130, 237, 238, and 239. The mean and standard deviation in the standard rectangle were calculated after each row (or set of rows) was removed by interpolating in the vertical direction using CLEAN. When the mean changed by less than 0.10 ADU/pixel, no further modifications were made. The mean of the overclocked area was subtracted as usual from the corresponding frame.

The overclock-subtracted dome flat-fields (12 per bandpass) were averaged in each bandpass. The mean bias frame was subtracted from each of the mean overclock-subtracted dome flat-fields. The mean dark frame was scaled down by the appropriate factors, 60/900 = 0.06667 for R, and 90/900 = 0.1000 for B, and the scaled mean dark frames were subtracted from the bias- and-overclock-subtracted dome flat-fields producing a mean bias-and- dark-corrected dome flat-field frames for each bandpass.

3.6 Sky Images

The sky images are integrations (900 seconds in R and 1200 seconds in B) of 'blank' areas of sky. These images are of course not truly vacant, but contain many faint stars and galaxies. The R images display interference fringes, since the chip acts as a thin film for wavelengths in the R bandpass. The fringes are believed to be due to a number of strong night sky emission lines in this region, in particular, neutral oxygen at 6300 Å and 6364 Å (see figure 3.1). These electromagnetic waves interfere constructively and destructively, according to the thickness of the chip at a given point, producing an interference pattern by the same mechanism which produces Newton's rings. By comparing different sky images, it could be seen qualitatively that the shape of the interference fringe pattern was not variable, although the intensity did vary slightly. The amplitude of the fringes above the local background is estimated to be less than 1%. No attempt was made to remove the fringes.

Two of the sky images were checked for large scale gradients by sampling 40 X 40 pixel squares at various locations. Over the whole image, a less than 2% change in the background was found horizontally, and the shape was consistent between images with a peak in the middle and a drop to both sides. A top to bottom decrease of less than

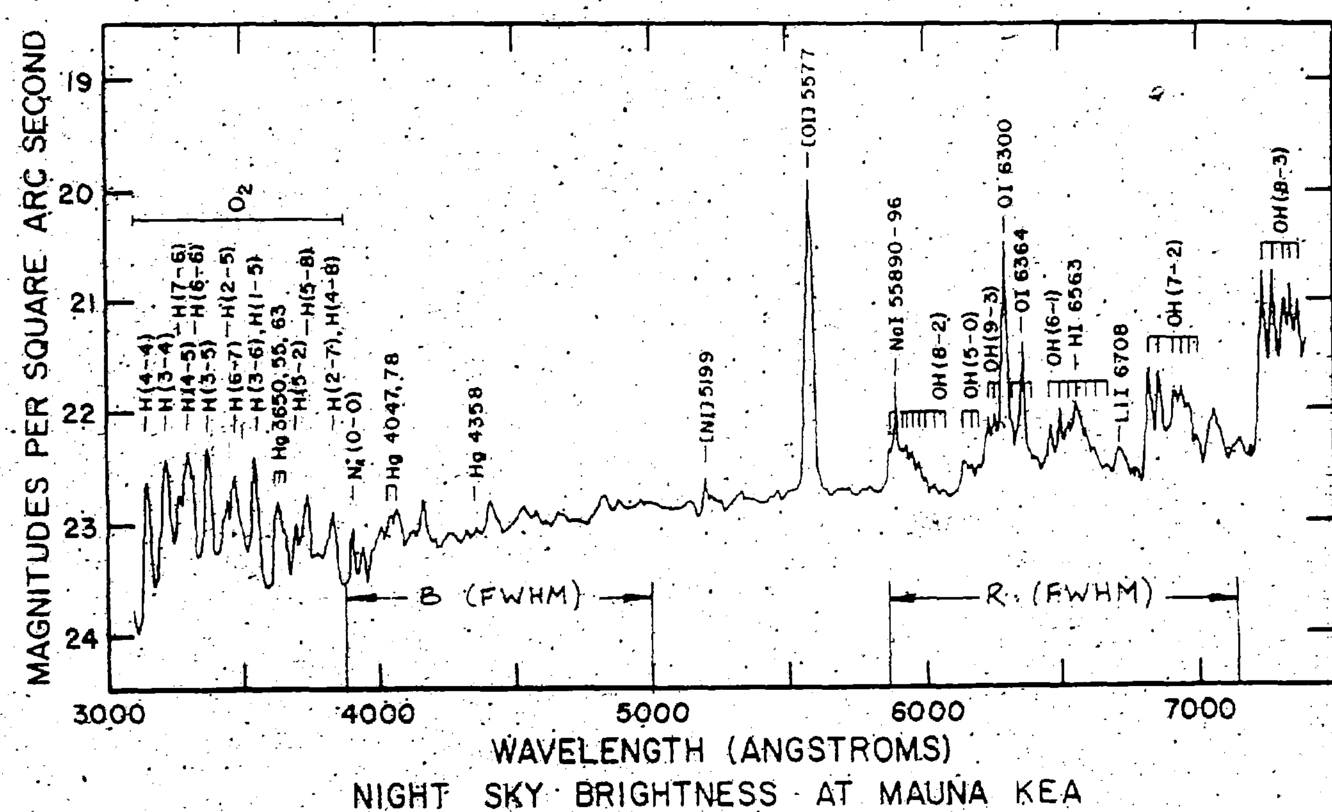

Figure 3.2. The spectrum of the night sky at Mauna Kea (Racine and Lelievre 1982).

4% was found. These gradients are probably due to large scale sensitivity variations, which are removed by the flat-fielding process described below.

At this stage some method of removing large unwanted objects (ie., stars and galaxies) was required. FUZH was developed for this purpose. The initial plan was to use FUZH to remove as many of the larger objects as possible and then use CLEANH to remove the smaller blemishes. The number of blemishes removed using FUZH sometimes ran as high as 60, requiring up to 4 hours of work. Fortunately, only 6 (of 13) sky images were cleaned this way before programme MEDFR was developed. MEDFR is capable of removing blemishes as large as the filter, thereby eliminating many of the smaller blemishes which previously had to be removed using FUZH. The typical filter size used was 21 X 21 pixels. This size was choosen so as to minimize the size of the unfiltered border, and to avoid the distortion of the halo gradient which would have resulted from the use of a larger filter. All sky images were recleaned, using FUZH to remove blemishes larger than 21 pixels square (typically 10 blemishes and 0.5 to 1 hour of work per image), followed by MEDFR to remove the smaller blemishes.

The overclocked areas showed no hot rows, but the ramp over the first 4 columns was present. The standard rectangle was used to determine the mean of the overclocked area of each image, and this was subtracted from the corresponding image. An average overclock-subtracted sky image was calculated for each bandpass (6 in R and 7 in B), and the mean bias frame was subtracted from each of these.

Recall that when cleaning the dark frames (using CLEANH and FUZH) the LEDs were excluded from treatment. MEDFR is not capable of excluding specified portions of an image. It therefore removes the LEDs. If unfiltered dark frames (with LEDs) were subtracted from filtered images (without LEDs), the result would be negative numbers at the location of the LEDs. This problem was solved by filtering the mean dark frame using the same filter size, discriminant, and weights as were used in filtering the sky images. The filtered mean dark frame, with appropriate scaling, was then subtracted from the bias- and- overclock-subtracted mean sky flat-fields.

Programme FLATR was used to correct the mean dark- and-bias-corrected sky images for areal non-uniformity of response (flat-fielded) using the mean dome flat-fields. The flat-fielding process consists of dividing the ADU count of each pixel of the image to be corrected by the ADU count of the corresponding pixel of a normalized flat-field frame. The flat-field is normalized by dividing each of its pixels by the average ADU count of the flat-field frame (Leach et.al. 1980). This may be expressed as,

$$I_i' = I_i / \{F_i / \langle F \rangle\} \qquad (3.1)$$

where, I_i' is the ith pixel of the corrected image,

I_i is the corresponding pixel in the uncorrected image,

F_i is the corresponding pixel in the flat-field frame,

and $\langle F \rangle = (1/N)\sum_i^N F_i$ is the average of the flat-field frame.

That this is in fact a correction for non-uniformity of response can be seen as follows. If we assume the chip images a uniform source, then the normalized flat-field gives for each pixel the factor by which it differs from the mean response of all pixels on the chip. If, for example, some pixel's normalized value is less than 1, then it has not responded as strongly as the 'mean pixel'. If the same pixel responds similarly during an image exposure then its ADU count will be lower than that of the 'mean pixel'. The correct ADU count is obtained by dividing by the normalized pixel, thereby increasing its ADU count so that it appears to have the same response as the 'mean pixel'.

The process of flat-fielding with the dome flat-fields does not completely remove all sensitivity variations, because the chip responds differently to the different spectral energy distributions of the high intensity lamp and the sky. Following Kormendy (1984) we used modified mean sky images to perform a second flat-fielding operation. The process of modifying the mean sky images involves dividing the image into 16 X 15 pixel rectangles and replacing the individual pixels with their average value over the rectangle (programme BLKAVG). This procedure has the disadvantage of smoothing out any real small-scale variations, but increases the overall signal-to-noise ratio (S/N) in the resulting image. This was desirable because of the low exposure level of typical sky images. The individual sky images were then flat-fielded with the appropriate smoothed mean sky flat-field, reducing the large scale variation to less than 1%.

The individual sky images were intended to be used to represent the sky background in the object images. However, direct subtraction of a treated individual sky image would significantly decrease the S/N of the resulting net object image. To avoid this we decided to model the sky with a two-dimensional second order polynomial (using programme POLYFT). It was assumed that the variation of the sky brightness over the chip was not sufficiently rapid to warrant a higher order polynomial.

3.7 Object Images

The object images in this study are 900^s and 1200^s integrations (in R and B respectively) of the galaxies being studied, and 60^s and 120^s integrations of the photometric calibration fields. These images suffer the same problems as the sky images (ie., interference fringes in R and a liberal sprinkling of stars and galaxies over the field) and were cleaned in basically the same manner. FUZH was used to remove the larger objects, and in some cases it was necessary to interpolate (vertically) over the hot rows 237 to 239. The overclocked area was cleaned and the mean ADU value within the standard rectangle determined in the usual manner.

These images were also filtered, but the filter severely distorted the bright cores of the programme galaxies. The distortion of the inner regions (less than 20 kpc from the centre in the case of NGC 6166) was obvious from visual inspection. In the case of NGC 6166, filtering resulted in the coalescence of the multiple nuclei and in the appearance of 'jet-like' structures radiating from the centre. A check of the average ADU/pixel value in a 10×10 pixel box showed that the difference between the filtered and unfiltered images was about 0.27% at 21 kpc from the centre of NGC 6166. To convince ourselves that the filtering had not affected the halo gradient, we took horizontal and vertical profiles through an image created by subtracting the filtered and unfiltered (but otherwise fully processed) versions of the same image. The profiles showed random scatter about zero, indicating that the filtering process had not distorted the large scale gradients outside the core.

The individual images were bias- and- dark-corrected, mean dome flat-fielded, and mean sky flat-fielded as usual. The final step involved the removal of the sky background. The first attempt at this involved subtracting the polynomial fit to the sky image which was closest both spatially and temporally to the object image. This was initially attempted, with apparent success, on R and B images of NGC 6166 (object:A332Y4; sky:C333Y4, object:A336Y4; sky:C335Y4). However, when the procedure was applied to a B image of the cD in A1413 (object:A322Y4; sky:C321Y4) it resulted in negative numbers over most of the image. Apparently the sky background was significantly variable ($\sim$5 to 6% of the sky) during and/or between these exposures. When this procedure was applied to a second R image of NGC 6166 (object:A130Y4; sky:C131Y4) the same problem occurred. The initial success with the other NGC 6166 images appears to have been fortuitous. The possibility that the sky background varied significantly during those integrations must be considered. Reduction of the calibration field images will provide a clear measure of the photometric quality of the sky.

Preliminary investigations of the type to be described in section 4.1 indicated that the sky level may have been reached on the images of the centre of NGC 6166. This provided another way of estimating the sky background. We calculated the average ADU count in a rectangle placed in the upper right corner (435,500,235,310 = 5016 pixels) of the treated (but not sky-subtracted) object image and in the same place on the polynomial representing the corresponding sky image. This area was choosen for the following reasons. The orientation of the galaxy on the images was such that the upper-right corner was the area farthest from the centre of the galaxy. Also, there was no apparent gradient due to the galaxy's halo in this area. The 'shape' of the sky, as represented by the polynomial, was assumed to remain constant and the polynomial was scaled by multiplying by the ratio of the two sky values. The scaling factors were: for C131Y4; 0.9438, C333Y4; 1.1010, C335Y4; 1.0588. The scaled polynomials were subtracted from the corresponding object images.

TABLE 3.1. Image Processing Programmes: Names, Authors, and Functions

Name (Author)	Function
CLEAN (1,4m)	Replaces a small area of an image using a specified value or a value interpolated from the pixels bordering the area.
CLEANH (1,2m,4m)	Replaces hot pixels with a local background value.
HUNTH (2)	Creates a file containing the coordinates of hot pixels (using same detection technique as CLEANH).
PIXH (2)	Compares files created by HUNTH and finds coordinates common to all files.
FUZH (2,3,4)	Removes large blemishes by two-dimensional interpolation.
MEDFR (2,3)	Removes blemishes using the median filter technique.
RECTR (3)	Performs statistics (mean, standard deviation, histograms, etc) in a rectangular area of an image.
DISH (3)	Displays an image produced by an RCA CCD.
ARITIR (4)	Performs an arithmetic operation on each pixel of an integer number image, producing a real number image.
AVR (3)	Computes the average of up to ten images.
SUBR (3)	Computes the difference of two images (pixel-by-pixel).
FLATR (3)	Flat-fields an image.
BLKAVG (4)	Heavily smoot[illegible] an image by averaging in blocks.
POLYFT (4)	Computes the coefficients of a second order, two-dimensional polynomial fit to an image and constructs a corresponding image file.
CONH (1)	Identifies pixels of similar brightness, and is ususally used to locate isophotes.

TABLE 3.1. (Continued)

Name(Author)	Function
SBPROF (4)	Delineates isophotes, allows ellipses to be fit to them by eye, and determines the average ADU/pixel value under the ellipses.
ELAVG1 (4)	Calculates the average ADU/pixel value under a single ellipse.
ELAVG2 (4)	Calculates the average ADU/pixel value between two ellipses if both ellipses lie completely in the image area.
ELAVG3 (4)	Calculates the average ADU/pixel value between two ellipses if one or both ellipses intersect the edge of the image.

Author notation: 1 = G. Collins
2 = G. A. Welch
3 = D. M. K. Welch
4 = J. W. B. Allwright
'm' beside a number means the author modified the programme only.

CHAPTER 4

RESULTS AND DISCUSSION

In section 4.1 the methods used in generating the surface brightness profiles by fitting ellipses to the approximate isophotes will be discussed, along with the method of normalizing the profiles. Section 4.2 contains a discussion and comparison of these profiles with previous work. Section 4.3 outlines plans for improving the reduction procedure.

4.1 Surface Brightness and Colour Profiles

Generating a surface brightness profile from the processed object images involves three steps: 1) the identification of pixels with ADU values within a given range (i.e., isophote generation), 2) fitting ellipses to isophotes by visual inspection, and 3) determining the mean surface brightness at the radial distance from the centre of the galaxy represented by the ellipse. This method assumes that elliptical isophotes are appropriate for cD galaxies on the basis that they are used satisfactorily in modelling the light distribution of elliptical galaxies. Note that this process uses image coordinates in units of pixels; the conversion to physical coordinates is made after the profile has been generated.

A more objective method of fitting ellipses using numerical methods has been developed by Young et al. (1979) and modified by Kent (1983). This method will be applied to our data in the future.

The initial attempts,at finding isophotes, or regions of similar brightness, used programme CONH. This programme essentially delineates an isophote by locating pixels which have an ADU count larger than a specified level, and which have at least one neighbour with a lower ADU count. This resulted in thin isophotes with fairly sharp edges in regions of rapidly changing ADU, but in broad isophotes with poorly defined edges in areas where the gradient was small.

The problem of ill-defined isophotes was partially solved by creating programme ISOPHT. This programme is a modification of CONH which allows the user to specify the range of ADU values used in defining the contour. This allows greater flexibility in generating isophotes. For example, when a particular ADU range generates too 'fuzzy' an isophote, a narrower range can be specified to sharpen it.

The next step involved fitting ellipses to the isophotes using the ellipse drawing routines (ELLS2I, ELL2, and ELSAVI). These programmes allow the parameters of an ellipse to be adjusted while the ellipse is visually fit to the isophote generated by ISOPHT.

At this point SBPROF was written for the purpose of combining the tasks described above and thereby reducing processing time. SBPROF first checks each pixel to determine if its ADU count lies within the range specified. If so, its location is stored in the output file which is then displayed on a TV monitor. An ellipse is then fit by eye to the resulting isophote. The ADU values of pixels in the object image corresponding to those forming the ellipse are then combined to derive a mean ADU/pixel value along the ellipse. The programme can also calculate the mean ADU/pixel value within an annulus defined by two non-intersecting ellipses (ELAVG1, ELAVG2, and ELAVG3). This option, which sacrifices radial resolution, is used to increase the S/N in regions of low signal.

SBPROF was used to derive surface brightness profiles from three images of NGC 6166, one in B (A332Y4) and two in R (A336Y4, A130Y4). The R image A336Y4 was analysed first. The isophote generating option was used to find pixels in the range 499 - 501 ADU. This was the largest ADU value used because at larger values the distortion due to filtering was greater than 1%. A single ellipse was fit to the resulting isophote, and the average under the ellipse determined. This process continued for isophotes separated by 50 ADU out to the 199 - 201 isophote, and at 20 ADU intervals thereafter out to the 99 - 101 ADU isophote. Annuli were used to generate the remainder of the profile. The coordinates of the centres of all the annuli were taken as the average of the coordinates of the previous 12 ellipses. The coordinates of the centres of the ellipses were within ± 3 pixels of their average. The ellipticity and position angle of the outermost ellipse was used for all annuli. The first six annuli were each 5 pixels wide and separated by 10 pixels. The remaining 11 annuli varied from 8 to 20 pixels wide.

The B surface brightness was determined from image A332SS using the same set of ellipses and annuli. Before this could be done the B and R images needed to be registered so that the coordinates of the ellipses and annuli referred to the same areas of the galaxy on both images. This was done by comparing the location of the peaks in the brightness distribution of two stars common to both images and in diagonally opposite corners of the images. As expected, this showed that the images differed only by a translation in both directions. The same technique of registration was used on the second red image, which served as a check on the systematic errors.

The results described so far are given in Table 4.1. Column (1) contains: for the first 12 entries, the semi-major axis in pixels of the best-fitting ellipse, and for the remaining 17 entries, the semi-major axes of the inner boundary of the annulus. Column (2) is the geometric mean of the semi-major and semi-minor axes of the best-fitting ellipse ($\sqrt{ab}$) to the power 0.25. For annuli, the axes of the ellipse midway between the inner and outer borders is used. This gives r which is used for ease of comparison with previous work and is calculated from the following:

$$r^{1/4} = \left\{ 0.417\ (R/2) \sqrt{1 - e}\ \ (187000/206265) \right\}^{1/4}, \qquad (4.1)$$

where 0.417 arcsec/pixel is the scale of the image, R is the major axis in pixels, e is the ellipticity, and 187,000 kpc is the distance to NGC 6166 (Thuan and Romanishin 1981). The factor $(R/2)\sqrt{1 - e} = \sqrt{ab}$ is derived from the definition of ellipticity, $(b/a) = 1-e$, and the fact that $a = (R/2)$. Columns (3) and (4) contain the instrumental surface brightness as functions of r in B and R respectively. These are calculated as follows:

$$\mu = -2.5 \log \left\{ 0.417^{-2}\ I \right\} + c', \qquad (4.2)$$

where I is the surface brightness in ADU/pixel in the B or R

TABLE 4.1. Instrumental b (A332Y4) and r (A336Y4, A130Y4) Surface Brightness and (b-r) Colour Profiles of NGC 6166.

a (1)	$r^{1/4}$ $(kpc)^{1/4}$ (2)	μ_b (mag/□) (A332Y4) (3)	μ_r (mag/□) (A336Y4) (4)	$\mu_b - \mu_r$ (mag/□) (5)	μ_r^c (mag/□) (A130Y4) (6)	$\mu_b - \mu_r^c$ (mag/□) (7)
46	1.97199	-7.79434	-8.59836	0.80402	-8.63793	0.84359
50	2.01310	-7.63443	-8.44406	0.80963	-8.48730	0.85287
54	2.04834	-7.50379	-8.31577	0.81198	-8.35776	0.85397
57	2.08299	-7.38554	-8.19355	0.80801	-8.23686	0.85132
64	2.14368	-7.18102	-7.98104	0.80002	-8.02677	0.84575
72	2.20357	-6.96942	-7.76253	0.79311	-7.82224	0.85282
86	2.29513	-6.68622	-7.46899	0.78277	-7.53477	0.84855
88	2.30018	-6.67921	-7.45633	0.77712	-7.52571	0.84650
97	2.34368	-6.54917	-7.32443	0.77526	-7.39599	0.84682
106	2.39149	-6.40416	-7.17514	0.77098	-7.24532	0.84126
120	2.45702	-6.20007	-6.97371	0.77364	-7.04645	0.84638
132	2.51602	-6.03057	-6.74783	0.71726	-6.86760	0.83703
140	2.56445	-5.88983	-6.55829	0.66846	-6.71869	0.82886
154	2.62712	-5.67722	-6.32594	0.64872	--------	--------
170	2.68951	-5.42155	-6.09708	0.67553	-6.26588	0.84433
186	2.74964	-5.19121	-5.86675	0.67554	-6.07849	0.88728
200	2.79920	-4.93811	-5.69780	0.75969	-5.87225	0.93414
215	2.84954	-4.70861	-5.49552	0.78691	-5.67924	0.97113
230	2.90199	-4.42392	-5.20410	0.77718	-5.46820	1.04428
240	2.93544	-4.26789	-5.02322	0.75533	-5.33651	1.06862
250	2.96489	-4.11011	-4.86590	0.75579	-5.18063	1.07052
260	2.99629	-3.93419	-4.69692	0.76273	-5.05618	1.12199
272	3.03218	-3.57157	-4.44409	0.87252	-4.86522	1.29365
286	3.06947	-3.26149	-4.16440	0.90291	-4.64914	1.38765
300	3.10669	-3.18216	-3.91280	0.73064	-4.58055	1.39839
315	3.14384	-2.41862	-3.63788	1.21926	-4.26252	1.84390
330	3.17973	-1.99699	-3.37272	1.37573	-4.19390	2.19691
345	3.21443	-1.45296	-3.00393	1.55097	-3.97906	2.52610
360	3.25355	-0.92717	-2.51500	1.58783	-3.80894	2.88177

band as calculated by SBPROF, $(0.417)^{-2}$ = 5.7508 pixels/(arcsec)^2 is the areal scale of the image, and c' is an additive constant to be determined below. Column (5) is the difference of columns (3) and (4), giving the instrumental colour (b-r). Column (6) is the instrumental surface brightness in R from the second image (A130Y4; superscript `c') and column (7) is the difference of columns (3) and (6).

Some method of normalizing our measurements was needed in order to compare our results with other work. Time did not permit processing the calibration fields, which would otherwise have been used to transform our measurements to the standard system. Instead, we normalized our photometry to existing photometry at one radial point of the galaxy in order to obtain the additive constant in equation (4.2).

Gallagher et al. (1980, Table 1) give the extinction and K- corrected colours, $(B-V)_o = 0.97$ and $(V-R)_o = 0.79$ at R_{eq} = 22 kpc, where R_{eq} is assumed to be the same as the geometric radius ($\sqrt{ab}$). Thuan and Romanishin (1981, figure 7) find μ_V = 22.40 mag arcsec^{-2} at the same radial distance. Assuming that the isophotes and isochromes have the same shapes, and disregarding the possible aperture smearing effects discussed by Valentijn (1983), the blue surface brightness at this distance is approximately,

$$\mu_B = (B-V)_o + \mu_V = 0.97 + 22.40 = 23.37 \text{ mag}/\square . \quad (4.3)$$

By interpolation between the entries for a = 64 and 72 pixels in column (3) of Table 4.1, μ_b = −7.11049. The correction to be added to the entries in column (3) is the difference of μ_B and μ_b ; ie.,

$$c' = \mu_B - \mu_b = 30.48 \text{ mag}/\square . \quad (4.4)$$

For the colour at R_{eq} = 22 kpc we find from Gallagher et al.,

$$(\mu_B - \mu_R)_G = (B-R)_o = (B-V)_o + (V-R)_o = 1.76 \text{ mag}/\square , \quad (4.5)$$

while according to Table 4.1 column(5), $\mu_b - \mu_r$ = 0.79772. The correction to be added to the entries in column (5) is therefore,

$$c'' = (\mu_B - \mu_R)_G - (\mu_b - \mu_r) = 0.96 \text{ mag}/\square . \quad (4.6)$$

The entries in column (4) are normalized by adding $c' - c''$. The same procedure is applied in normalizing column(6) of Table 4.1. These profiles are tabulated in Table 4.2. Column (1) is the same as column (2) of Table 4.1, column (2) is the normalized B surface brightness as a function of $r^{1/4}$, column (3) is the same for R; column (4) is the normalized (B-R) profile, column (5) is the R profile of the second red image (A130Y4), and column (6) is the difference of columns (3) and (5). For $r^{1/4} < 2.6$ (kpc)$^{1/4}$ the difference is $\lesssim$ 11 %. For greater galactocentric distances, the difference gets progressively larger. Column (7) is the normalized colour profile derived from the second red image.

TABLE 4.2. Normalized B (A332Y4) and R (A336Y4, A130Y4) Surface Brightness and (B-R) Colour Profiles of NGC 6166.

$r^{1/4}$ (kpc$^{1/4}$) (1)	μ_B (mag/□") (A332Y4) (2)	μ_R (mag/□") (A336Y4) (3)	$\mu_B-\mu_R$ (mag/□") (4)	μ_R^c (mag/□") (A130Y4) (5)	$\mu_R-\mu_R^c$ (mag/□") (6)	$\mu_B-\mu_R^c$ (mag/□") (7)
1.9720	22.68566	20.91936	1.76630	20.93018	-0.01082	1.75548
2.0131	22.84557	21.07366	1.77191	21.08081	-0.00715	1.76476
2.0483	22.97621	21.20195	1.77426	21.21035	-0.00840	1.76586
2.0830	23.09446	21.32417	1.77029	21.33125	-0.00708	1.76321
2.1437	23.29898	21.53668	1.76230	21.54134	-0.00466	1.75764
2.2036	23.51058	21.75519	1.75539	21.74587	0.00241	1.76471
2.2951	23.79378	22.04873	1.74505	22.03334	0.01539	1.76044
2.3002	23.80079	22.06139	1.73940	22.04240	0.01899	1.75839
2.3437	23.93083	22.19329	1.73754	22.17212	0.02117	1.75871
2.3915	24.07584	22.34258	1.73326	22.32279	0.01979	1.75305
2.4570	24.27993	22.54401	1.73592	22.52166	0.02501	1.75827
2.5160	24.44943	22.76989	1.67954	22.70051	0.06938	1.74892
2.5645	24.59017	22.95943	1.63074	22.84942	0.11001	1.74075
2.6271	24.80188	23.19178	1.61010	--------	-------	-------
2.6895	25.05845	23.42064	1.63781	23.30223	0.11841	1.75622
2.7496	25.28879	23.65097	1.63782	23.48962	0.16135	1.79917
2.7992	25.54189	23.81992	1.72197	23.69586	0.12406	1.84602
2.8495	25.77139	24.02220	1.74919	23.88887	0.13292	1.88252
2.9020	26.05308	24.31362	1.73946	24.09991	0.20388	1.95317
2.9354	26.21211	24.49450	1.71761	24.23160	0.26290	1.98051
2.9649	26.36989	24.65182	1.71807	24.38748	0.26434	1.98241
2.9963	26.54581	24.82080	1.72501	24.51193	0.30858	2.03388
3.0322	26.90843	25.07363	1.83480	24.70289	0.37074	2.17953
3.0695	27.21851	25.35332	1.86519	24.91897	0.43435	2.29954
3.1067	27.29784	25.60492	1.69292	24.98756	0.61736	2.31028
3.1438	28.06138	25.87984	2.18154	25.30559	0.57425	2.75579
3.1797	28.48301	26.14500	2.33801	25.37421	0.77079	3.10880
3.2144	29.02704	26.51379	2.51325	25.58905	0.92474	3.43799
3.2536	29.55283	27.00272	2.55011	25.75917	1.24355	3.79366

4.2 Discussion

The normalized B and R surface brightness profiles are presented in figures 4.1 and 4.2, respectively. Included in these plots are Oemler's V-band data as given in Thuan and Romanishin (1981 figure 7). These data, and the deVaucouleurs law fit by Thuan and Romanishin (1981), have been normalized by adding $(B-V)_o = 0.97$ in B and subtracting $(V-R)_o = 0.79$ in R (Gallagher et al. 1980). In both cases our profiles seem to agree with Oemler's out to roughly $r^{1/4} = 2.6\ (\mathrm{kpc})^{1/4}$, or $r \sim 45$ kpc. Farther from the centre our profiles depart radically from Oemler's. The rapid decline exibited by our surface brightness profiles for $r > 45$ kpc is probably caused by our method of determining the sky background. Our assumption that the sky has been reached in the upper-right corner of the object images has probably resulted in the subtraction of not only sky light but some of the galaxy's light as well. To test this we determined the semi-major axis of the first annulus to intersect the region used to scale the sky. The intensity of the galaxy at the corresponding distance, as given by Oemler's profile, was subtracted from each of Oemler's data points. The resulting profile is given by the solid squares in figure 4.1. It follows our observed profile quite closely. This indicates that our method of determining the sky background has probably produced the rapid decline in our profiles.

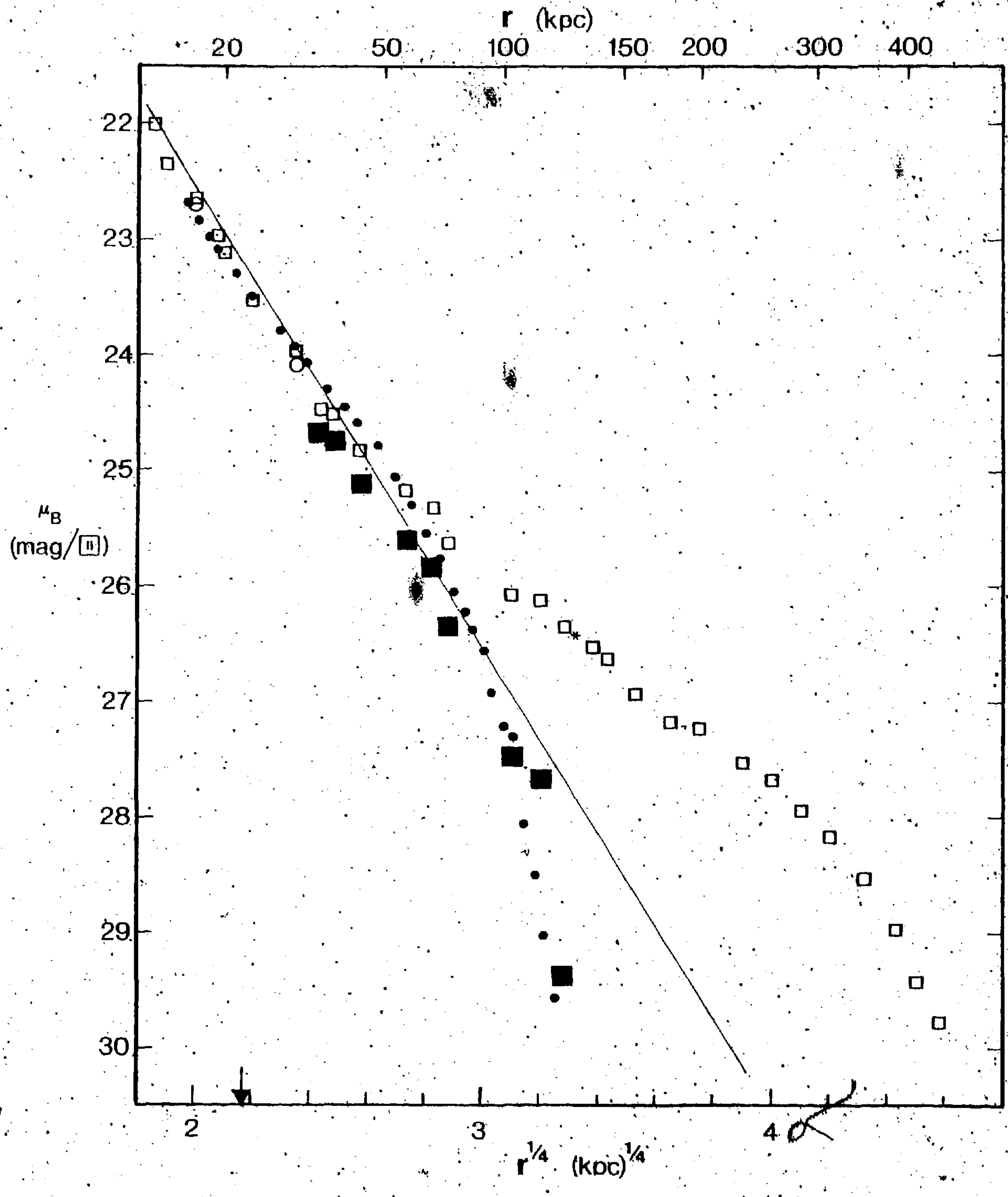

Figure 4.1. The B surface brightness profile of NGC 6166 from A332Y4 (•), normalized at the point indicated by the arrow, to Oemler's V-band photometry (□). The solid line is a deVaucouleur law fit by Thuan and Romanishin (1981) to Oemler's data. The solid squares represent some of Oemler's data reduced by the intensity given by the asterisk. For clarity, Oemler's data havebeen shifted down vertically by 0.97 mag/arcsec^2.

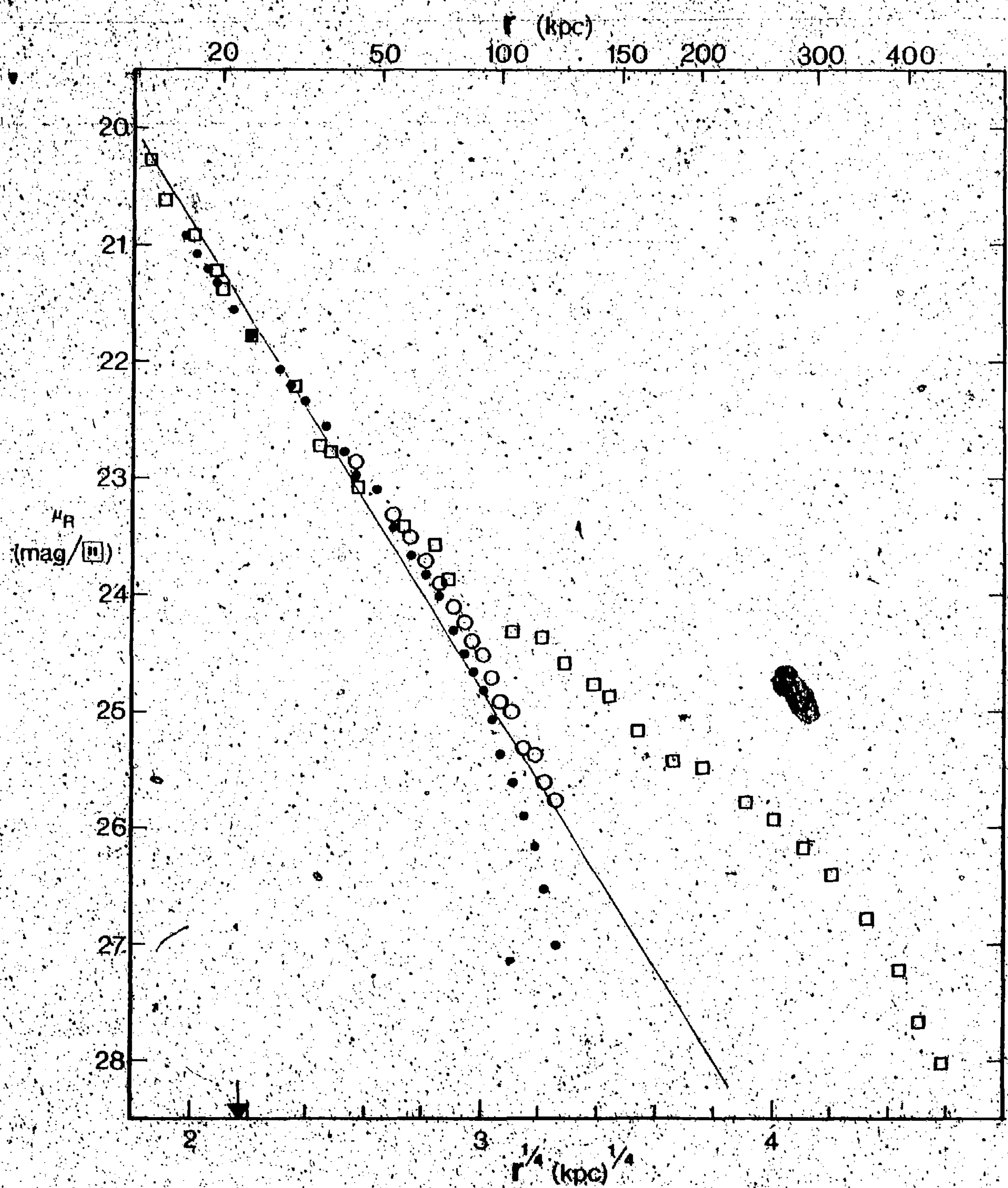

Figure 4.2. The R surface brightness profile of NGC 6166 from A336Y4 (●) and A130Y4 (○) normalized as in Figure 4.1. The squares and the solid line are as in Figure 4.1 except that they have been shifted up vertically by 0.79 mag/arcsec^2.

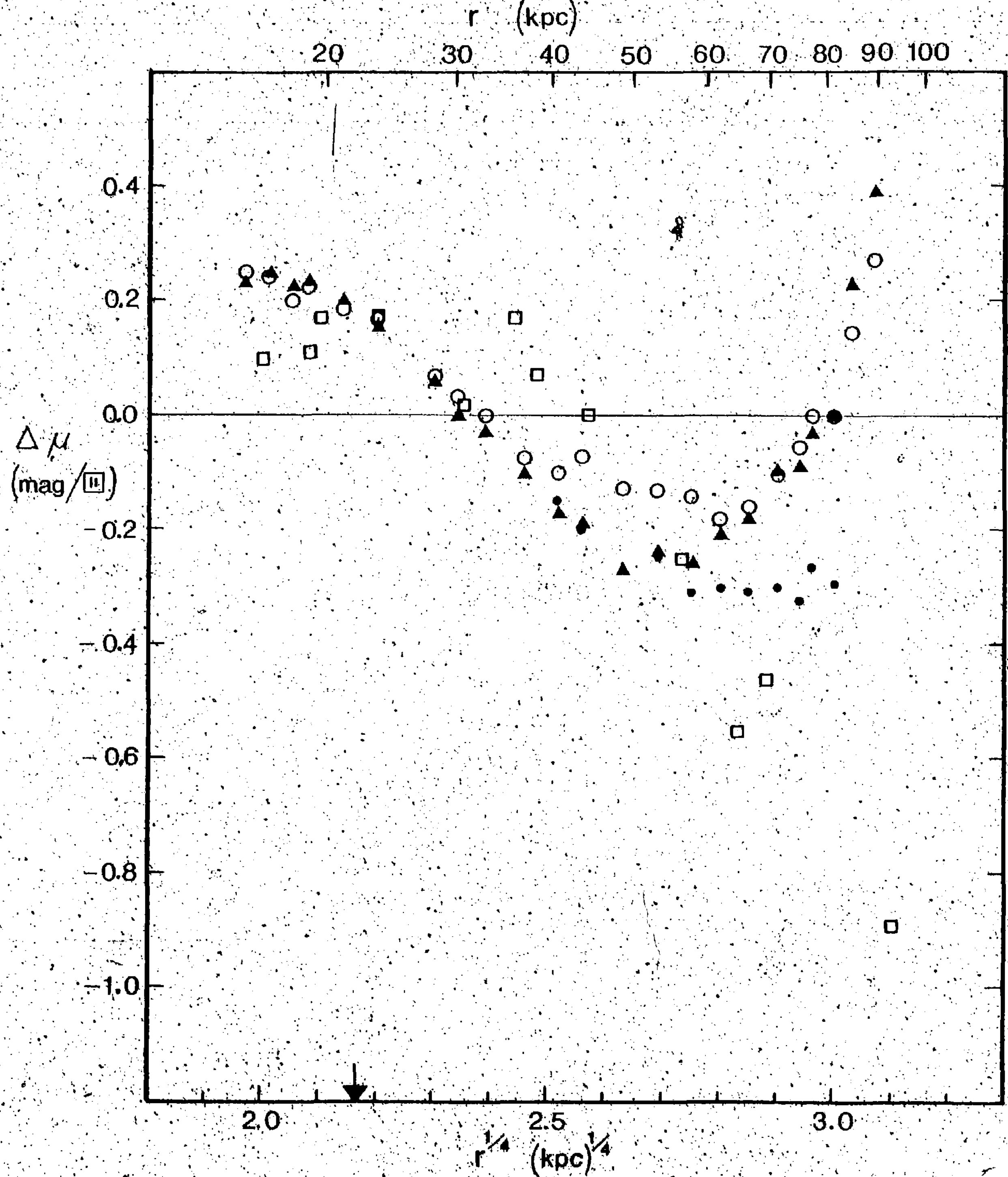

Figure 4.3. The differences between the various observed surface brightness profiles and the deVaucouleurs law given in Figures 4.1 and 4.2. Open circles are for R (A336Y4), solid circles for R (A130Y4), triangles for B (A332Y4), and squares are for Oemler's V-band data.

The profile from the second red image (A130Y4) is plotted as the open circles (○) in Figure 4.2, where it differs from the A336Y4 profile by more than 10%. As can be seen from Table 4.2 and Figure 4.2 the profiles from the two red images are in fairly good agreement (ie., 0.10 mag difference) for $r^{1/4} < 2.6$. For $r^{1/4} > 2.6$ the difference becomes progressively greater.

In order to more clearly show the detailed structure of the profiles for $r^{1/4} < 3.0$ the differences between the various profiles and the deVaucouleurs law are plotted in figure 4.3. On this scale the departure of our profiles for $r^{1/4} > 2.6$ from the trend shown by Oemler's data is more obvious. The trends displayed by each profile continue for $r^{1/4} > 3.0$. Our profiles tend to be much smoother than Oemler's, indicating that our observations are less noisy. This plot also shows that the deVaucouleurs law published by Thuan and Romanishin (1981) does not fit the observed profiles very well. According to Oemler's profile the halo begins at $\sim r^{1/4} = 2.6$. Our profiles indicate that it begins closer to the centre of the galaxy at $\sim r^{1/4} = 2.35$. However, part of this difference could be due to the normalization of our observations.

The (B-R) colour profiles derived from the two red images are given in figure 4.4. For clarity the data for $r^{1/4} > 3.0\ (\mathrm{kpc})^{1/4}$ are not plotted. The A130Y4 data (•) show that the colour of the galaxy becomes bluer by ~ 0.03 mag for $2.0 < r^{1/4} < 2.6$, and then reddens rapidly for $r^{1/4} > 2.6$. The A336Y4 data (O) show that the colour becomes bluer by ~ 0.04 mag for $2.0 < r^{1/4} < 2.4$, then drops sharply by ~ 0.125 mag between $r^{1/4} = 2.4$ and 2.6. This is followed by a steep reddening trend similar to the A130Y4 data. To model the effect of our treatment of the sky on the colour profiles we calculated the magnitude difference between Oemler's profile (figure 4.1 □) and Oemler's profile modified as described above (figure 4.1 ■). These differences represent the effect of subtracting galaxy light in addition to the light of the sky. The differences were plotted as a function of distance and a smooth curve was fit by eye to the points. The curve was normalized to $(B\text{-}R) = 1.77$ at $r^{1/4} = 2.0$, and plotted as the solid triangles in figure 4.4. This profile shows what would be obtained if all the error introduced by our method of determining the sky level entered in the B bandpass. The actual curve cannot be any steeper than shown because the error in the R bandpass is in the same sense as in the B bandpass, and therefore reduces the steepness of the curve. This result shows, however, that the overall magnitude and sense of the observed colour gradient could result from our method of

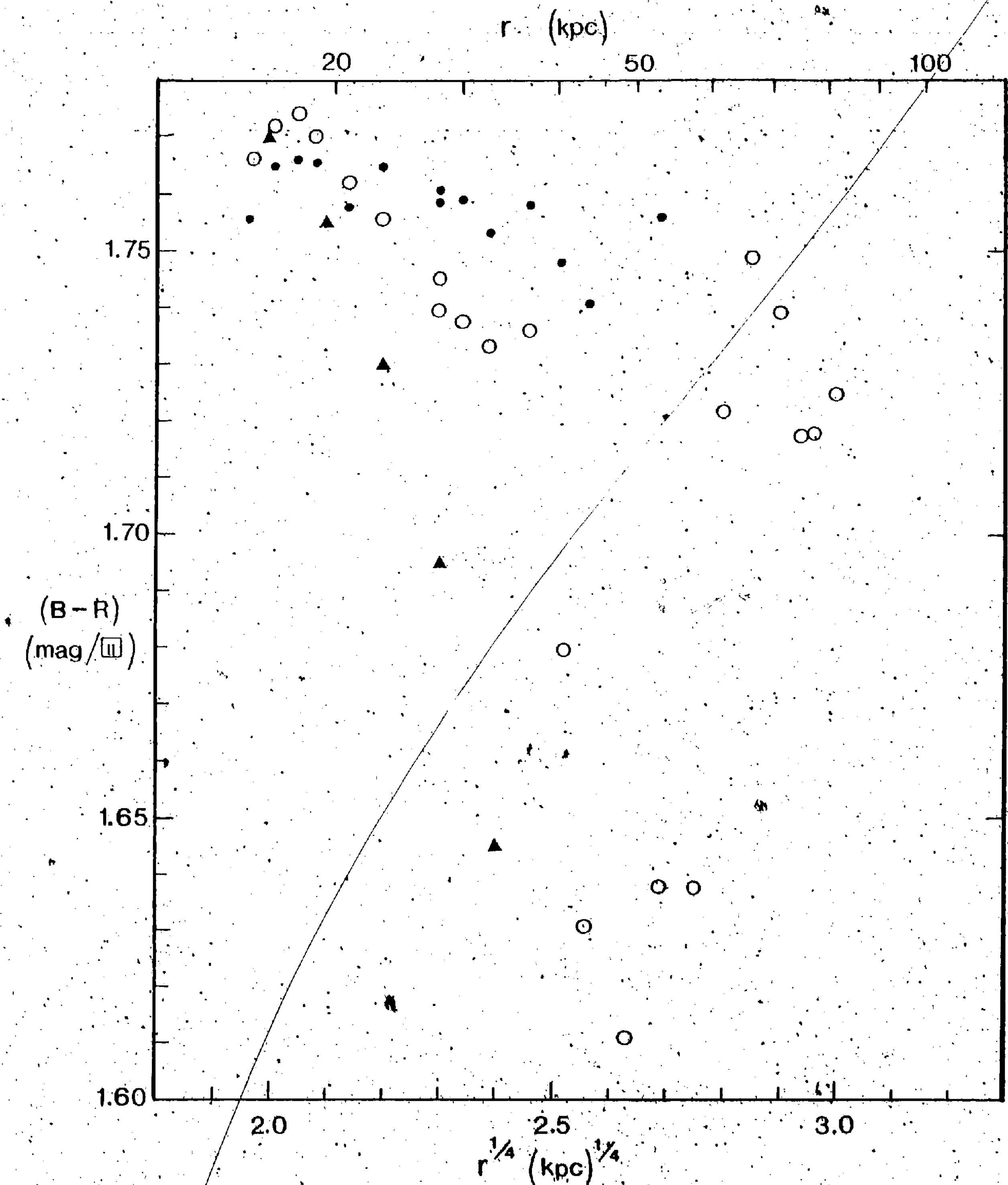

Figure 4.4: The B-R colour profiles for NGC 6166 from the blue image A332Y4 and the red images: A336Y4 (O), and A130Y4(•). The triangles represent the model discussed in the text.

determining the sky level. On the other hand, the model cannot reproduce the complicated structure of the observed profiles, for example, the ~0.01 mag bump at $r^{1/4} = 2.05$. This kind of structure may in fact be real, thus justifying comparison of these profiles with other work.

The arithmetic average of the two (B-R) colour profiles is plotted in figure 4.5. The error bars represent the difference between the two profiles. Also plotted are colour profiles taken from Gallagher et al. (1980) and Valentijn (1983). Gallagher et al. give a (B-V) colour profile of NGC 6166, and Valentijn gives the average (B-V) values of a sample of 6 cDs (not including NGC 6166) at galactocentric distances of 50 and 80 kpc. The (B-V) values were crudely transformed to (B-R) using the relationship between (B-V) and (V-R) for giant stars given by Johnson (1966). This relation was normalized to the (B-V) vs. (V-R) data for elliptical galaxies from Gallagher et al. (1980, Table 1), by subtracting 0.15 mag in (B-V). In the inner region of our average profile ($2.0 < r^{1/4} < 2.45$) the colour becomes bluer by 0.03 mag. This change is similar to the overall trend displayed by the data of Gallagher et al. The change in colour over the inner region is larger than the typical error in the same region. The trend displayed in the inner regions confirms the general conclusion of previous observational studies, and the prediction of the

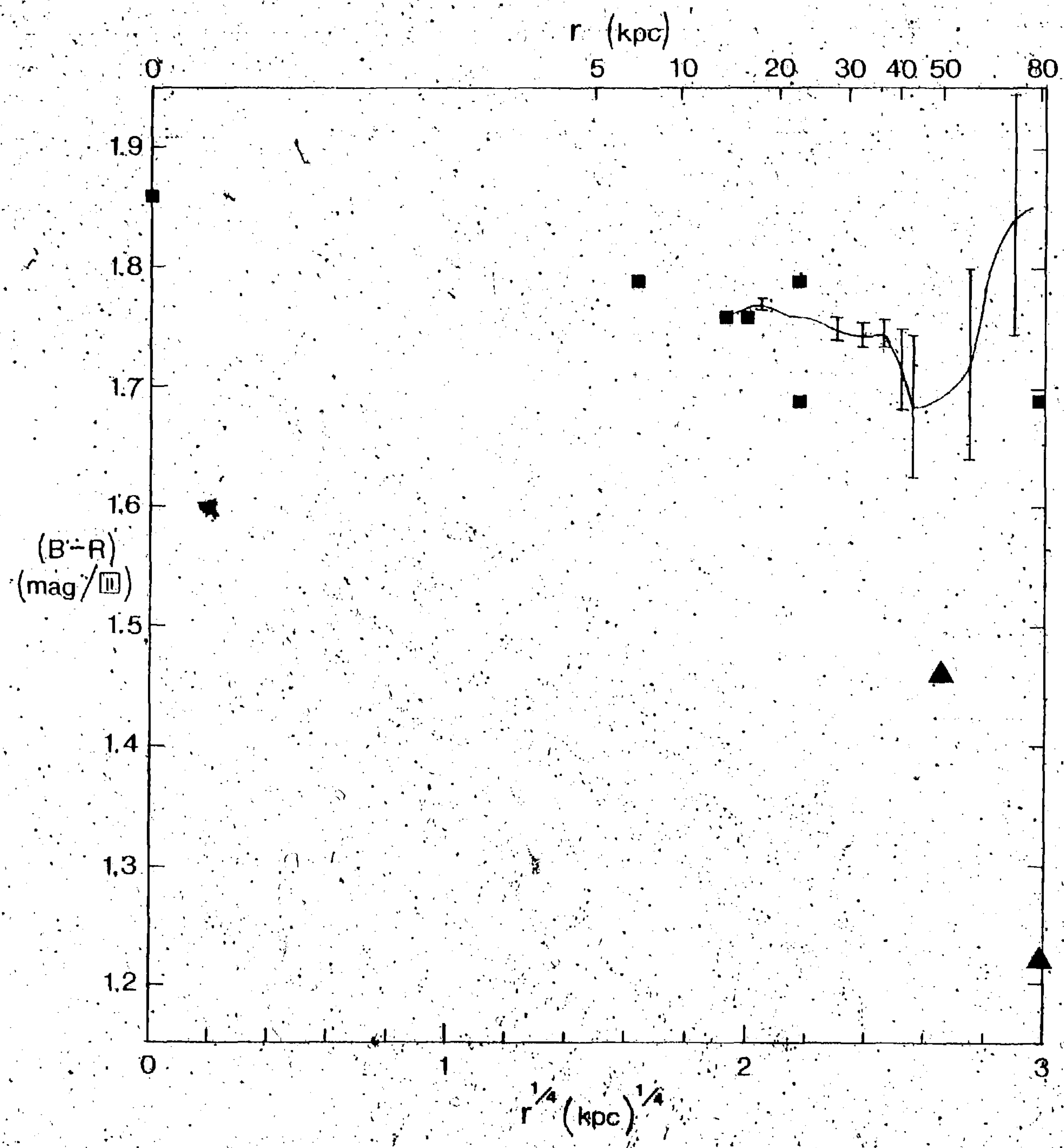

Figure 4.5. The average of the two colour profiles in Figure 4.4 is given by the smooth curve. The error bars represent the difference between the profiles. The normalized data of Gallagher et al. (1980) are given by the squares, and that of Valentijn (1983) by the triangles.

tidal debris and the cooling intracluster medium models, that cD galaxies become bluer at larger galactocentric distances.

The sharp drop to bluer colours between $r^{1/4} = 2.45$ and 2.55, and the subsequent rapid reddening, may be artifacts of our method of determining the sky level. However, it is interesting to note that if the rapid drop between $r^{1/4} = 2.45$ and 2.55 were extended it would give colours similar to Valentijn's. At this time we cannot infer anything further about the region beyond $r^{1/4} = 2.45$.

4.3 Future Improvements in Data Reduction

Future efforts will concentrate on developing a method of determining the sky background corrections. Three possibilities are given below.

We have examined only a small subset of the data obtained at the CFHT. Therefore, we will first process the complete data set using the original technique of subtracting an unscaled polynomial fit to a sky image.

Alternatively, we could determine the sky level on the short exposures of the central regions of the galaxies (eg., A110Y4), and force the profiles obtained from the short exposures to fit those obtained from the long exposures. The sky background on the halo images would be fixed by forcing the halo and central image profiles to agree in the region where the images overlap. There may, however, be a problem with a low signal-to-noise ratio in the short exposures.

If the halo images have not reached the outer halo then it may be possible to approximate the sky background using a suitable portion of the halo images. The sky background on the central images can then be fixed by forcing the profiles generated by the central and halo images to agree in the region where the two images overlap.

Another improvement will involve developing a more objective method of fitting ellipses to isophotes (Young et al. 1979 and Kent 1983). This will hopefully determine the run of ellipticity and position angle of the isophotes. Also, the calibration images will be used to determine the extinction and transformation coefficients.

CHAPTER 5

SUMMARY

B and R CCD images of NGC6166 in A2199 and the anonymous cD galaxy in A1413 have been obtained using the CFH 3.6m telescope. A systematic procedure for the processing of CCD images has been developed. It involves subtracting the bias level introduced by the electronics, subtracting the thermal background, removing unwanted objects and blemishes, and correcting for areal sensitivity variations across the CCD.

Surface brightness profiles in B and R for NGC 6166 were obtained by determining the average ADU/pixel values in concentric elliptical annuli, and were normalized using the photometry of Gallagher et al.(1980), and of Oemler (1976) as presented by Thuan and Romanishin (1981). Our profiles agree with Oemler's out to $\sim$45 kpc from the centre. Beyond this point our profiles drop rapidly compared to Oemler's. The sky background was found to vary significantly. The method used to determine the sky level probably produced the rapid decline displayed by our profiles.

The (B-R) colour profile becomes bluer by 0.03 mag between galactocentric distances of roughly 16 and 33 kpc. Beyond 33 kpc the profile shows a sharp dip to the blue

followed by a rapid reddening. Some of these trends, in particular the rapid reddening may be caused by our method of determining the sky level. The 0.03 mag decline between 16 and 33 kpc is qualitatively consistent with the observations of Gallagher et al. (1980) and with the predictions of both the tidal debris and cooling ICM models of cD galaxy formation. However, these results are tentative, pending examination and reduction of the complete data set.

APPENDIX Journal of Observations

DATE : 3/4 May 1984.

File Name (1)	UT h m (2)	Object (3)	Integ-ration sec (4)	Filter (5)	ST h m s (6)	RA 1950 h m (7)	DEC 1950 ° ' (8)
C101Y4	05 22	Dome	60	R	09 49 45		
C102Y4	05 28	Dome	60	R	09 55 42		
C103Y4	05 32	Dome	90	B	09 59 05		
C104Y4	05 36	Dome	90	B	10 02 50		
B105Y4	05 39	Bias			10 06 04		
B106Y4	05 40	Bias			10 07 26		
A107Y4	07 09	N4147	30	B	11 36 11	12 09.1	18 37.0
A108Y4	07 19	N4147	90	B	11 46 47	12 09.1	18 37.0
A109Y4	07 26	N4147	60	R	11 53 43	12 09.1	18 37.0
A110Y4	07 43	A1413	60	R	12 10 49	11 54.3	23 29.7
A111Y4	07 52	A1413	60	R	12 19 47	11 54.2	23 29.8
A112Y4	07 58	A1413	600	R	12 25 20	11 54.2	23 29.8
C113Y4	08 20	A1413s1	900	R	12 47 52	11 53.0	23 49.8
B114Y4	08 39	Bias			13 07 12		
B115Y4	08 41	Bias			13 08 18		
B116Y4	08 42	Bias			13 09 23		
A117Y4	08 49	A1413h	900	R	13 16 51	11 54.0	23 29.8
C118Y4	09 13	A1413s2	900	R	13 40 25	11 54.2	23 01.8
A119Y4	09 34	A1413	1200	B	14 01 50	11 54.2	23 29.8
C120Y4	10 01	A1413s1	1200	B	14 29 13	11 53.0	23 49.8
A121Y4	10 25	A1413h	1200	B	14 53 02	11 54.0	23 29.8
C122Y4	10 49	A1413s2	1200	B	15 17 17	11 54.2	23 01.8
B123Y4	11 14	Bias			15 41 51		
A124Y4	11 16	N4147	120	B	15 43 47	12 09.2	18 37.2
A125Y4	11 20	N4147	120	R	15 47 44	12 09.2	18 37.2
B126Y4	11 24	Bias			15 52 38		
B127Y4	11 26	Bias			15 54 14		
A128Y4	12 07	N6166	60	R	16 35 52	16 28.0	39 35.2
A129Y4	12 35	N6166	60	R	17 03 38	16 28.0	39 35.2
A130Y4	12 40	N6166	900	R	17 08 48	16 28.0	39 35.3
C131Y4	13 02	N6166s1	900	R	17 30 05	16 28.0	39 20.3
C132Y4	13 19	N6166s1	1200	B	17 47 36	16 28.0	39 20.3
A133Y4	13 43	N6166	1200	B	18 11 13	16 28.0	39 35.3
B134Y4	14 05	Bias			18 34 08		
B135Y4	14 08	Bias			18 37 09		

3/4 May 1984 continued;

File Name (1)	UT h m (2)	Object (3)	Integ-ration sec (4)	Filter (5)	ST h m s (6)	RA 1950 h m (7)	DEC 1950 ° ' (8)
A136Y4	14 19	M92	120	B	18 47 43	17 16.4	43 04.1
A137Y4	14 25	M92	120	R	18 53 15	17 16.4	43 04.1
A138Y4	14 29	M92	60	R	18 57 23	17 16.4	43 04.1
A139Y4	14 31	M92	60	B	18 59 53	17 16.4	43 04.1
B140Y4	14 34	Bias			19 02 17		
B141Y4	14 35	Bias			19 03 22		
B142Y4	14 36	Bias			19 04 26		
B143Y4	14 37	Bias			19 05 31		
B201Y4	14 44	Bias			19 12 31		
B202Y4	14 45	Bias			19 13 20		
B203Y4	14 46	Bias			19 14 26		
B204Y4	14 47	Bias			19 15 30		
C205Y4	14 48	Dome	1	B	19 17 10		
C206Y4	14 52	Dome	90	B	19 21 13		
C207Y4	14 57	Dome	90	B	19 25 56		
C208Y4	15 06	Dome	90	B	19 35 03		
C209Y4	15 09	Dome	90	B	19 38 14		
C210Y4	15 12	Dome	90	B	19 41 03		
C211Y4	15 16	Dome	60	R	19 44 32		
C212Y4	15 18	Dome	60	R	19 47 00		
C213Y4	15 20	Dome	60	R	19 49 12		
C214Y4	15 22	Dome	60	R	19 51 21		
D215Y4	15 22	Dark	1				
D216Y4		Dark	900				
D217Y4		Dark	900				
D218Y4		Dark	900				
D219Y4		Dark	900				
D220Y4		Dark	900				
D221Y4		Dark	900				
D222Y4		Dark	900				
D223Y4		Dark	900				
D224Y4		Dark	900				
D225Y4		Dark	900				
D226Y4		Dark	900				
D227Y4		Dark	900				

3/4 May 1984 continued;

File Name (1)	UT (2)	Object (3)	Integration sec (4)	Filter (5)	ST (6)	RA 1950 (7)	DEC 1950 (8)
D228Y4		Dark	900				
D229Y4		Dark	900				
D230Y4		Dark	900				
D231Y4		Dark	900				
D232Y4		Dark	900				
D233Y4		Dark	900				
D234Y4		Dark	900				
D235Y4		Dark	900				

DATE: 4/5 May 1984

File Name (1)	UT h m (2)	Object (3)	Integration sec (4)	Filter (5)	ST h m s (6)	RA 1950 h m (7)	DEC 1950 ° ' (8)
B301Y4	04 59	Bias			09 30 07		
B302Y4	05 00	Bias			09 31 08		
B303Y4	05 01	Bias			09 32 17		
B304Y4	05 02	Bias			09 33 25		
D305Y4	05 04	Dark	900		09 35 32		
C306Y4	05 28	Dome	60	R	09 59 42		
C307Y4	05 31	Dome	60	R	10 01 55		
C308Y4	05 33	Dome	60	R	10 04 27		
C309Y4	05 36	Dome	90	B	10 07 37		
C310Y4	05 39	Dome	90	B	10 10 19		
C311Y4	05 42	Dome	90	B	10 13 15		
C312Y4	05 45	Dome	10	B	10 16 15		
C313Y4	05 47	Dome	90	B	10 17 49		
A314Y4	06 34	N4147	60	B	11 05 34	12 09.2	18 37.0
A315Y4	06 42	N4147	120	B	11 13 00	12 09.2	18 37.0
A316Y4	06 47	N4147	120	R	11 18 11	12 09.2	18 37.0
A317Y4	06 57	A1413	60	R	11 28 12	11 54.4	23 29.8
A318Y4	07 01	A1413	120	R	11 32 25	11 54.2	23 29.7
A319Y4	07 07	A1413	900	R	11 38 01	11 54.2	23 29.7
A320Y4	07 26	A1413s1	900	R	11 57 27	11 53.0	23 49.8
A321Y4	07 43	A1413s1	1200	B	12 14 16	11 53.0	23 49.7
A322Y4	08 07	A1413	1200	B	12 39 05	11 54.2	23 29.8
B323Y4	08 33	Bias			13 05 03		
B324Y4	08 35	Bias			13 06 27		
A325Y4	08 36	N4147	120	B	13 08 05	12 09.2	18 37.0
A326Y4	08 41	N4147	120	R	13 12 47	12 09.2	18 37.0
D327Y4	08 45	Dark	900		13 16 51		
A328Y4	09 22	M92	60	R	13 53 33	17 16.4	43 04.5
A329Y4	09 28	M92	60	B	13 59 56	17 16.4	43 04.4
A330Y4	09 34	N6166	1200	B	14 05 58	16 28.0	39 35.3
A331Y4	10 01	N6166	120	B	14 33 22	16 28.0	39 35.7
A332Y4	10 05	N6166	1200	B	14 36 55	16 28.0	39 35.7
C333Y4	10 28	N6166s1	1200	B	14 59 37	16 28.0	39 20.7
C335Y4	10 49	N6166s1	900	R	15 21 06	16 28.0	39 20.6
A336Y4	11 07	N6166	900	R	15 39 29	16 28.0	39 35.7

4/5 May 1984 continued:

File Name (1)	UT h m (2)	Object (3)	Integ- ration sec (4)	Filter (5)	ST h m s (6)	RA 1950 h m (7)	DEC 1950 ° ' (8)
B337Y4	11 24	Bias			15 56 14		
A338Y4	11 29	N4147	120	R	16 01 32	12 09.2	18 37.0
A339Y4	11 34	N4147	120	B	16 05 54	12 09.2	18 37.0
B340Y4	11 37	Bias			16 09 26		
A401Y4	11 48	N6166	120	B	16 20 33	16 27.9	39 35.2
A402Y4	11 55	N6166h	1200	B	16 26 59	16 28.2	39 35.2
C403Y4	12 19	N6166s2	1443	B	16 50 52	16 26.6	39 40.2
A404Y4	12 47	N6166h	900	R	17 18 58	16 28.2	39 35.2
C405Y4	13 05	N6166s2	900	R	17 37 38	16 26.6	39 40.3
B406Y4	13 23	Bias			17 55 16		
A407Y4	13 26	M92	60	R	17 58 58	17 16.4	43 03.3
A408Y4	13 30	M92	60	R	18 02 34	17 17.4	43 03.6
A409Y4	13 33	M92	60	B	18 05 15	17 16.4	43 03.6
B410Y4	13 35	Bias			18 07 51		
A411Y4	13 39	N6166	120	B	18 11 25	16 27.9	39 35.0
A412Y4	13 44	N6166h	1200	B	18 16 41	16 28.2	39 34.9
C413Y4	14 06	N6166s2	1200	B	18 39 07	16 26.6	39 40.2
A414Y4	14 31	M92	60	B	19 03 22	17 16.4	43 03.4
A415Y4	14 33	M92	60	R	19 06 06	17 16.4	43 03.4
A416Y4	14 38	M92	30	R	19 10 56	17 16.5	43 09.0
A417Y4	14 40	M92	30	B	19 13 02	17 16.5	43 09.0
B418Y4	14 42	Bias			19 14 59		
B419Y4	14 44	Bias			19 16 25		
C420Y4	14 47	Dome	90	B	19 20 11		
C421Y4	14 50	Dome	90	B	19 23 08		
C422Y4	14 53	Dome	90	B	19 26 04		
C423Y4	14 57	Dome	60	R	19 29 21		
C424Y4	14 59	Dome	60	R	19 31 47		
C425Y4	15 01	Dome	60	R	19 34 13		
D501Y4	15 27	Dark	900		19 59 47		
D502Y4		Dark	900				
D503Y4		Dark	900				
D504Y4		Dark	900				
D505Y4		Dark	900				
D506Y4		Dark	900				
D507Y4		Dark	900				
D508Y4		Dark	900				
D509Y4		Dark	900				
D510Y4		Dark	900				

REFERENCES

Abell, G. O. 1958, Ap. J. Suppl., 3, 211.

Albert, C. E., White, R. A., and Morgan, W. W. 1977, Ap. J., 211, 309.

Bautz, L. P., and Morgan, W. W. 1970, Ap. J. (Letters), 162, L149.

Brownrigg, D. R. K. 1984, Commun. of the Assoc. for Comput. Machinery, 27, 807.

Christian, C. A. 1984, CFHT CCD and FOCAS User's Manual (Hawaii:Canada-France-Hawaii Telescope Corporation).

Christian, C. A., Adams, M., Barnes, J. V., Butcher, H., Hayes, D. S., Mould, J. R., and Siegel, M. 1985, Pub. A. S. P., 97, 363.

Cowie, L. L., and Binney, J. 1977, Ap. J., 215, 723.

de Vaucouleurs, G. 1948, Ann. d'Ap., 11, 247.

Fabian, A. C., Ku, W. H.-M., Malin, D. F., Mushotzky, R. F., Nulsen, P. E. J., and Stewart, G. C. 1981, M.N.R.A.S., 196, 35p.

Fabian, A. C., and Nulsen, P. E. J. 1977, M.N.R.A.S., 180, 479.

Fabian, A. C., Nulsen, P. E. J., and Canizares, C. R. 1982, M.N.R.A.S., 201, 933.

Gallagher, J. S., Faber, S. M., and Burstein, D. 1980, Ap. J., 235, 743.

Hausman, M. A., and Ostriker, J. P. 1978, Ap. J., 224, 320.

Heckman, T. M. 1981, Ap. J., 250, L59.

Johnson, H. L. 1966, Ann. Rev. Astr. Ap., 4, 193.

Jones, C., and Forman, W. 1984, Ap. J., 276, 38.

Kent, S. M. 1983, Ap. J., 266, 562.

King, I. R. 1966, A. J., 71, 64.

Kormendy, J. 1984, private communication.

Leach, R. W., and Gursky, H. 1979, Pub. A. S. P., 91, 855.

Leach, R. W., Schild, R. E., Gursky, H., Madejski, G. M., Schwartz, D. A., and Weekes, T. C. 1980, Pub. A. S. P., 92, 233.

Leir, A. A., and van den Bergh, S. 1977, Ap. J. Suppl., 34, 381.

Matthews, T. A., Morgan, W. W., and Schmidt, M. 1964, Ap. J., 140, 35.

Minkowski, R. 1961, A. J., 66, 558.

Morbey, C., and Morris, S. 1983, Ap. J., 274, 502.

Morgan, W. W. 1958, Pub. A. S. P., 70, 364.

Morgan, W. W., Kayser, S., and White, R. A. 1975, Ap. J., 199, 545.

Morgan, W. W., and Lesh, J. R. 1965, Ap. J., 142, 1364.

Murphy, H. P., Schild, R. E., and Weekes, T. C. 1983, M.N.R.A.S., 202, 1127.

Oemler, A. 1973, Ap. J., 180, 11.

Oemler, A. 1976, Ap. J., 209, 693.

Ostriker, J. P., and Hausman, M. A. 1977, Ap. J., 217, L125.

Ostriker, J. P., and Tremaine, S. D. 1975, Ap. J., 202, L113.

Racine, R., and Lelievre, G. 1982, CFHT Observers Manual (Hawaii:Canada-France-Hawaii Telescope Corporation).

Rees, M. 1985, Remarks made at a Conference on Galaxy Formation, University of Toronto, June 19-21.

Richstone, D. O. 1975, Ap. J., 200, 535.

Richstone, D. O. 1976, Ap. J., 204, 642.

Rood, H. J., and Sastry, G. N. 1971, Pub. A. S. P., 83, 313.

Sarazin, C. L., and O'Connell, R. W. 1983, Ap. J., 268, 552.

Stewart, G. C., Fabian, A. C., Jones, C., and Forman, W. 1984, Ap. J., 285, 1.

Strom, K. M., and Strom, S. E. 1978a, A. J., 83, 73.

Strom, S. E., and Strom, K. M. 1978b, A. J., 83, 732.

Strom, K. M., and Strom, S. E. 1978c, A. J., 83, 1293.

Thuan, T. X., and Romanishin, W. 1981, Ap. J., 248, 439.

Valentijn, E. A. 1983, Astr. Ap., 118, 123.

Valentijn, E. A., and Bijleveld, W. 1983, Astr. Ap., 125, 223.

Young, P. J., Sargent, W. L. W., Kristian, J., and Westphal, J. A. 1979, Ap. J., 234, 76.

CURRICULUM VITAE

NAME:	James William Bentley Allwright
PLACE OF BIRTH:	Montreal, Quebec, Canada.
DATE OF BIRTH:	November 26, 1956.
POST-SECONDARY EDUCATION:	Saint Mary's University, Halifax, Nova Scotia. 1978-1983 B. Sc. (Honours)
	Saint Mary's University, Halifax, Nova Scotia. 1983-1985 M. Sc.
HONOURS AND AWARDS:	Achievement Scholarship, Saint Mary's University. 1981-1983
	N.S.E.R.C. Undergraduate Summer Research Award, Saint Mary's University. 1981-1983
	N.S.E.R.C. Postgraduate Scholarship, Saint Mary's University 1983-1985
EXPERIENCE:	Summer Research Assistant, Department of Astronomy, Saint Mary's University. 1981-1983
	Laboratory Demonstrator, Department of Physics, Saint Mary's University. 1980-1982
	Laboratory Instructor, Department of Physics, Saint Mary's University. 1982-1984
PUBLICATIONS:	"Development of an Image Display System for Astronomical Data", B.Sc. Thesis, Allwright, J.W.B., Saint Mary's University, 1983.
	"New Observations of Six RV Tauri and SRd Variable Stars", DuPuy, D.L., Dawson, D.W., Allwright, J.W.B., and Africano, J., Pub. A. S. P., 95, 427, 1983.